General Disclaimer

One or more of the Following Statements may affect this Document

- This document has been reproduced from the best copy furnished by the organizational source. It is being released in the interest of making available as much information as possible.

- This document may contain data, which exceeds the sheet parameters. It was furnished in this condition by the organizational source and is the best copy available.

- This document may contain tone-on-tone or color graphs, charts and/or pictures, which have been reproduced in black and white.

- This document is paginated as submitted by the original source.

- Portions of this document are not fully legible due to the historical nature of some of the material. However, it is the best reproduction available from the original submission.

CR-137815

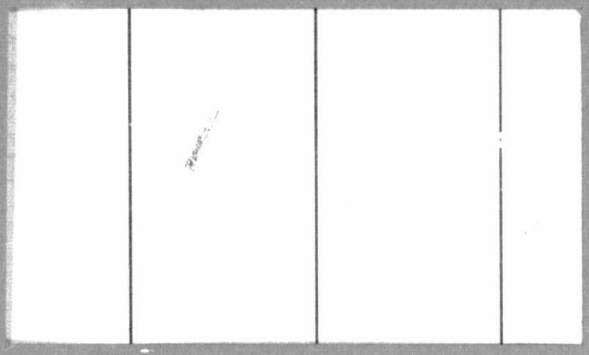

AEROELASTIC AND STRUCTURES RESEARCH LABORATORY

MASSACHUSETTS INSTITUTE OF TECHNOLOGY

CAMBRIDGE, MASS.

Use of Active Control Systems to Improve Bending and Rotor Flapping Responses of a Tilt Rotor VTOL Airplane

H. Philip Whitaker
Yi Cheng

ASRL TR 183-1 October 1975

Use of Active Control Systems to Improve Wing Bending and Rotor Flapping Responses of a Tilt Rotor VTOL Airplane

H. Philip Whitaker
Yi Cheng

October 1975

Prepared under NASA Grant NSG-2044 by the Aeroelastic and Structures Research Laboratory, Department of Aeronautics and Astronautics, Massachusetts Institute of Technology

for

Ames Research Center
National Aeronautics and Space Administration

ACKNOWLEDGEMENT

This report was prepared under OSP Project 82266 sponsored by NASA-Ames Research Center through National Aeronautics and Space Administration Grant number NSG-2044.

The publication of this report does not constitute approval by the NASA of the findings and conclusions contained herein. It is published only for the exchange and stimulation of information.

TABLE OF CONTENTS

ABSTRACT

This report summarizes the results of an analytical study of the use of active control systems for the purpose of reducing the root mean square response of wing vertical bending and rotor flapping to atmospheric turbulence for a tilt-rotor VTOL airplane. Only the wing/rotor assembly has been considered so that results of a wind tunnel test program would be applicable in a subsequent phase of the research. The capabilities and limitations of simple single feedback configurations were identified, and the most promising multi-loop feedback configurations were then investigated.

Design parameters were selected so as to minimize either wing bending or rotor flapping response. Within the constraints imposed by practical levels of feedback gains and complexity and by considerations of safety, reduction in response due to turbulence of the order of 30 to 50 per cent are predicted using the rotor longitudinal cyclic and a trailing edge wing flap as control effectors.

LIST OF ILLUSTRATIONS

List of Illustrations (Cont)

LIST OF TABLES

Chapter I

INTRODUCTION

This report summarizes a study of the use of automatic control systems to improve the response characteristics of the coupled modes of a tilt-rotor VTOL airplane. The study is an extension of research performed by the M.I.T. Aeroelastic and Structures Research Laboratory under the sponsorship of the Ames Research Center of the National Aeronautics and Space Administration (NASA), and that research provided the data base for the analysis of the automatic control systems described in this report (see Reference 1). Since correlation of experimental wind tunnel data with theoretical analyses was contemplated as the second phase of the preliminary research, Reference 1 considered only an assembly consisting of the prop-rotor mounted on a cantilever wing which corresponded to the available wind tunnel model. Two prototype rotor systems were available.

The study of control systems was motivated by the desire to reduce fatigue loads and to improve ride qualities by reducing the responses of rotor flapping and wing bending to atmospheric gust excitation. Additional interest was generated from the fact that the characteristics of the system modes change with speed, and at very high speed some of the modes approach instability (Reference 2). The possibility exists that the use of automatic controls can increase the stability margin of the wing-rotor system at high speed. The available manpower and time for the control studies precluded investigating the complete airplane response characteristics. Because of the complexity of the theoretical model of the wing/rotor combination, it was also considered to be premature to expend much effort on the full aircraft case until experimental verification of the wing/rotor model was obtained. The initial control studies have concentrated on the Bell rotor system which uses a gimballed stiff in-plane rotor.

The use of active automatic control systems for these purposes is predicated upon the assumption that devices exist which can exert the

required forces or moments upon either the wing or the rotor, or both, in such a fashion that the dynamic response of the wing/rotor system to gust excitation can be changed as desired. If one wishes, for example, to prevent vertical bending displacements of the wing due to a vertical gust, one needs to exert a force that opposes that displacement. In general it is not possible to eliminate the bending displacement unless one can predict the arrival of the disturbance force, since there will be dynamic lags in sensing the bending and in applying the corrective force. However one can decrease the amount of bending by increasing the effective bending stiffness and by damping the resultant oscillatory motions so that the motion decays faster. To do the former calls for as large a corrective force per unit bending displacement as possible while the latter calls for increasing the damping ratio of the oscillatory mode. If the control device is not an effective producer of force in the desired sense, the control system's capability is correspondingly reduced.

With the tilt-rotor vehicle, the available control devices are the blade collective and cyclic controls. A collective pitch change produces very little resultant vertical force when the rotor is tilted to the cruise configuration. Longitudinal cyclic control does produce effective vertical forces on the wing. These forces arise both as direct aerodynamic forces (induced drag) and as reactions to coupled motions in the other degrees of freedom. Lateral cyclic is an ineffective producer of vertical force. There is a further possibility of using wing trailing edge flaps, although that might involve a wing redesign effort. Motion of a wing flap of course directly affects the lift on the wing. The rotor blade cyclic controls also directly affect the flapping motion of the rotor through changes in lift on the blades.

Since atmospheric turbulence is a random process that can only be described statistically, the criteria for performance have been taken to be the root mean square values, (RMS), of the wing vertical bending coordinate, q_1, and of the rotor flapping coordinates, β_{1c} and β_{1s}. The performance capability of the control system is then indicated by the

percentage reduction in the (RMS) level when using the control system over that of the rotor wing system without the control system.

Method of approach

To synthesize an automatic control system configuration which will be effective and at the same time practical to implement, a parameter optimization approach has been employed. With such an approach a control system configuration (sensors, signal paths, signal compensation and control actuation devices) is specified on the basis of known availability of sensors and control system components. The various design parameters which are under the control of the designer can then be established by using a digital computer program that selects the parameter set which will achieve the desired performance. In this case it is the set that minimizes the (RMS) value of the desired output quantity for a specified spectrum of gust input. With this tool the performance capabilities and limitations of simple systems can be established, and additional feedback signal paths can be added as needed to achieve the desired performance. Concurrently with the optimization computations, root locus and Bode diagrams are used to obtain greater insight into how a particular feedback configuration modifies the system's static and dynamic characteristics in achieving the performance levels obtained. Importance throughout the study has been placed upon obtaining the simplest control system that will produce effective results.

Chapter II

THE WING/ROTOR ASSEMBLY

The wing/rotor assembly has been described in detail in Reference 1. Only the gimballed rotor has been considered in this report. Figure II-1 has been taken from that reference and is a schematic representation of the assembly pictured as a wind tunnel model. That reference showed that acceptable accuracy could be achieved considering only the nine lowest frequency modes of response of this dynamic system. These are coupled response modes, but they can be identified as dominantly associated with either the rotor or the wing as follows: a rotor blade collective flapping mode, a low frequency blade flapping mode, a high frequency blade flapping mode, a symmetric blade lagging mode, a low frequency blade lagging mode, and a high frequency blade lagging mode; and wing vertical bending, chordwise bending, and torsion modes.

The theoretical data for the wing/rotor system are summarized in Appendix A. The state matrices and transfer functions are presented there for a flight condition of 250 knots at sea level. The data presented in the coefficient matrices corresponds to a time scaling which is equivalent to nondimensionalizing the frequencies by dividing by rotor rotational angular velocity, 48.9 radian/sec or 458 RPM. That is convenient from an aerodynamic point of view. For control system design the rotor frequency is of no more significance than other component frequencies, and one is typically interested in the transient response as a function of time on a one-to-one scale. Accordingly the transfer functions are listed with the nondimensionalization removed. Frequencies are expressed in (radians/second) and time in seconds.

The transfer functions relating the rotor blade longitudinal flapping, β_{1c}, and the wing vertical bending coordinate, q_1, give the pole-zero configurations shown in Figure II-2. The collective lagging and the high frequency lagging rotor modes are off the scale of Figure II-2 (see the transfer function data). The gust will primarily excite the wing bending

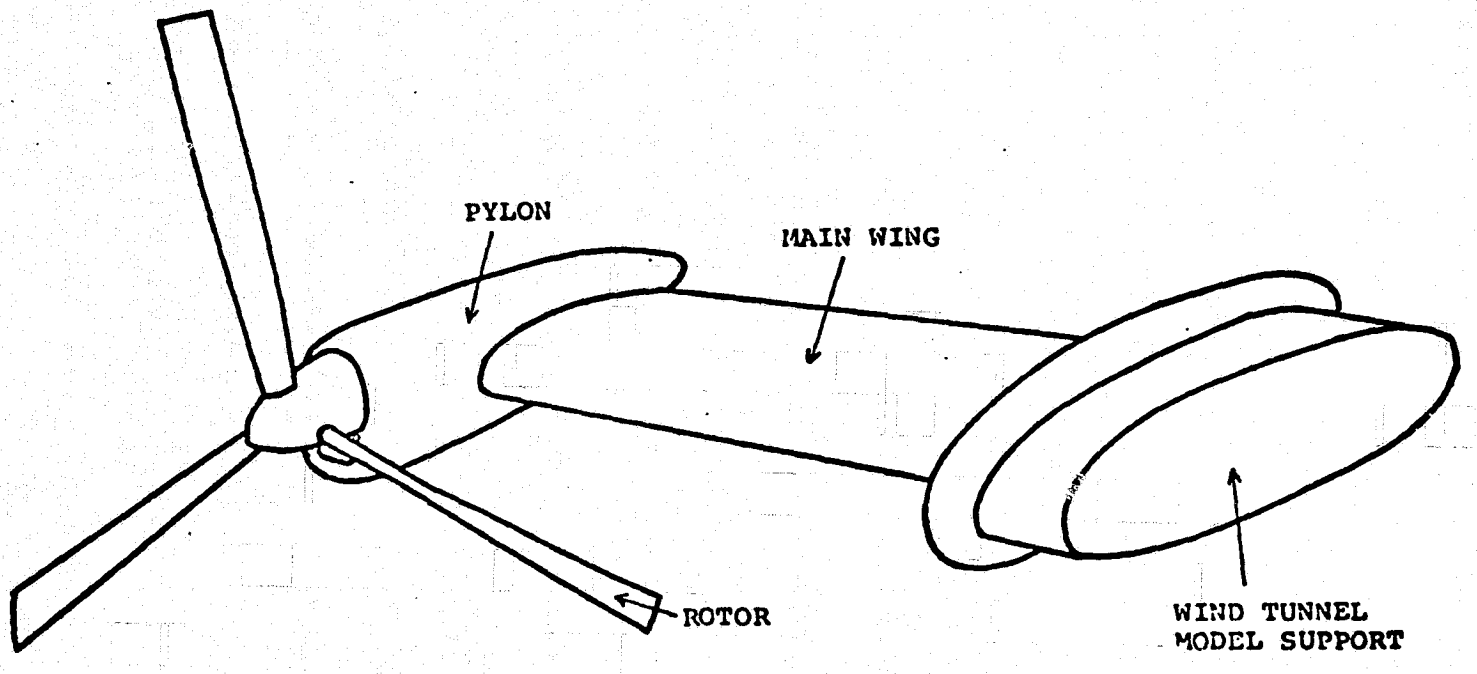

Figure II-1. Proprotor/Wing Assembly. Configuration for Cruise Flight.

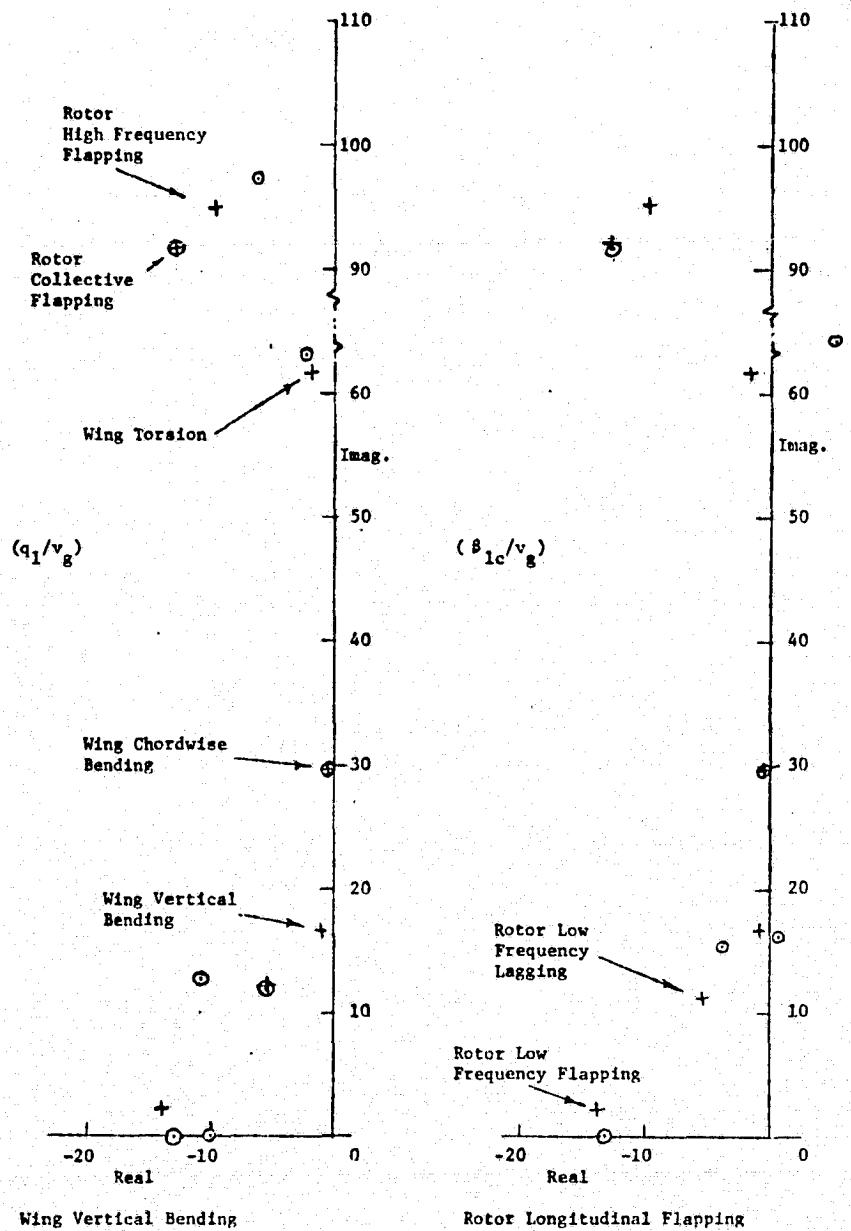

Figure II 2. Wing/rotor Assembly Transfer Function Pole-Zero Configuration; Input-nondimensional vertical gust velocity. 250 knot, sea level. Data: Appendix A.

mode in the bending response since approximate pole-zero cancellation occurs with the other modes. Similarly Figure II-2 predicts that in addition to the wing vertical bending mode and the low frequency rotor modes, the wing torsion mode will contribute to the rotor flapping response.

The assumed model for atmospheric turbulence is given in Appendix B. The bandwidth associated with the gust spectrum is approximately 1.4 rad/sec at a forward speed of 422 ft/sec (129 meters/sec). The turbulence can be modelled by assuming that white noise is fed to a filter that has frequency response characteristics that shape the noise so as to have the desired power spectral density. Such a filter would have two real poles at -0.747 and a real zero at -0.457 under the assumption that the gust characteristic length were 422 feet. That is the spectrum that has been used for all calculations of the (RMS) responses of the systems discussed in this report.

If one considers that a qualitative indication of the transient excitation of the response modes could be obtained by using the impulse response of the shaping filter as the input to the control systems, the time history of the filter impulse response would be as shown in Figure II-3a as curve A. It was intended that such an input be used as the time history of a representative pulse of vertical gust velocity so that some physical feel for the excitation of the response modes could be obtained. Unfortunately, due to a computer data input error that was not discovered until it was too late to obtain corrected data, the transient pulse time history that has been used corresponds to curve B of Figure II-3a. Thus all transient pulse time response data used curve B of Figure II-3a as the input. The frequency response of the two filters is presented in Figure II-3b. It is seen that filter B has a higher bandwidth (2.4 rad/sec) and greater amplitude ratio at all frequencies, and thus one would expect the transient pulse corresponding to it to produce greater high frequency excitation. Since the higher bandwidth input should be conservative and since only a qualitative evaluation was desired, it was decided to include the transient time histories using the input of curve B of Figure II-3a rather than to remove all transient pulse response data from the report. It is again em-

phasized that the above mentioned error applies only to the transient pulse data, and that the (RMS) level predictions were obtained using the correct power spectral density for the turbulence.

The input to the filter for Figure II-3a is a unit impulse. Since the static sensitivity of the filter is one, the total area under the response curve is unity. If one assumed that the nondimensionalized gust velocity (v_g/V), were represented by the shaped pulse of Figure II-3a, the corresponding response of the wing/rotor assembly is presented in Figure II-4. Shown in the figure are the responses of the wing vertical bending coordinate, the rotor longitudinal flapping coordinate, and the rotor lateral flapping coordinate. It is obvious that the wing vertical bending mode dominates the bending coordinate response as would be expected. The mathematical model being used predicts a period of 0.38 seconds and a damping ratio of 0.044 for this mode. The rotor blade cyclic flapping response exhibits excitation of several modes. Over the initial portion of the flapping response, the high frequency flapping mode is evident. The wing bending mode is present and is more noticeable on the lateral cyclic flapping response. The wing torsion mode can also be observed and is more evident on the longitudinal cyclic response. The wing torsion mode has a period of 0.102 seconds and a damping ratio of 0.025. The high frequency blade flapping mode has a period of 0.067 seconds and a damping ratio of 0.10.

Note that the general shape of the responses is similar to the pulse input with the response modes contributing oscillatory components superimposed. The bandwidth of the gust spectrum is low relative to the frequencies of the response modes. Thus the low frequency characteristic of the response in bending and flapping is generally in phase with the gust input.

When one examines the response to the random turbulence input, the ratio of the (RMS) value of wing vertical bending to the (RMS) value of nondimensional vertical gust velocity is found to be 0.178 (radian/radian). The bending coordinate here is the vertical bending displacement divided by the wing semispan, and the vertical gust velocity has been divided by

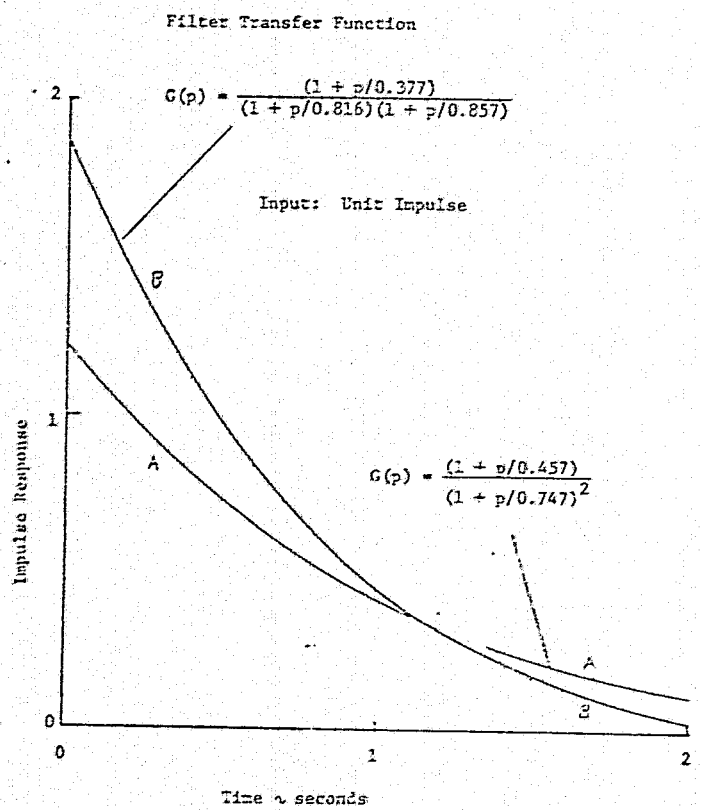

(a) Transient Shaped Pulse of Vertical Gust Velocity

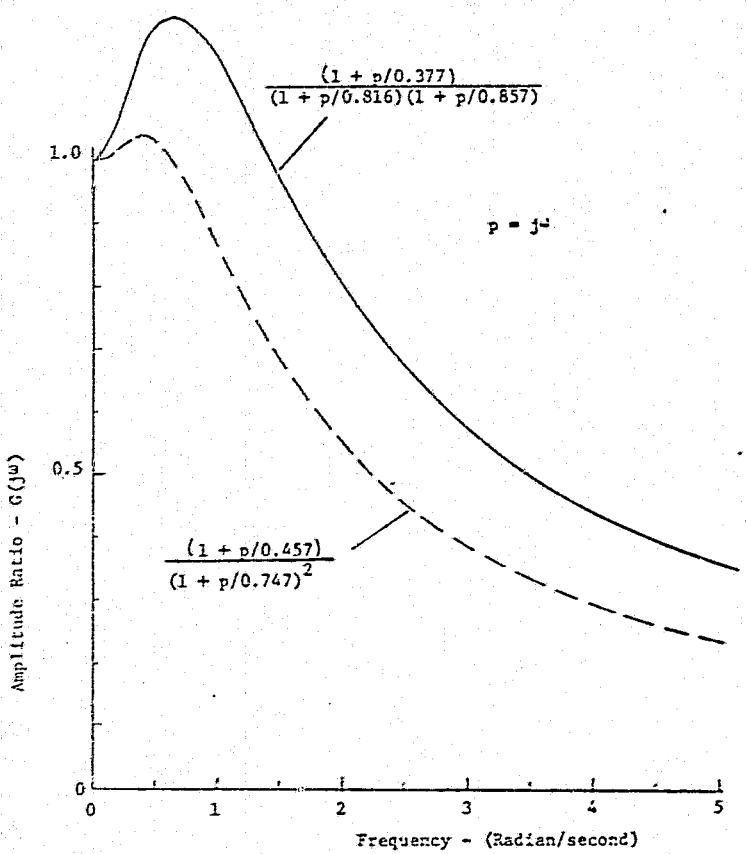

(b) Filter Frequency Response

Figure II-3. Representative Shaped Pulses of Vertical Gust Velocity.

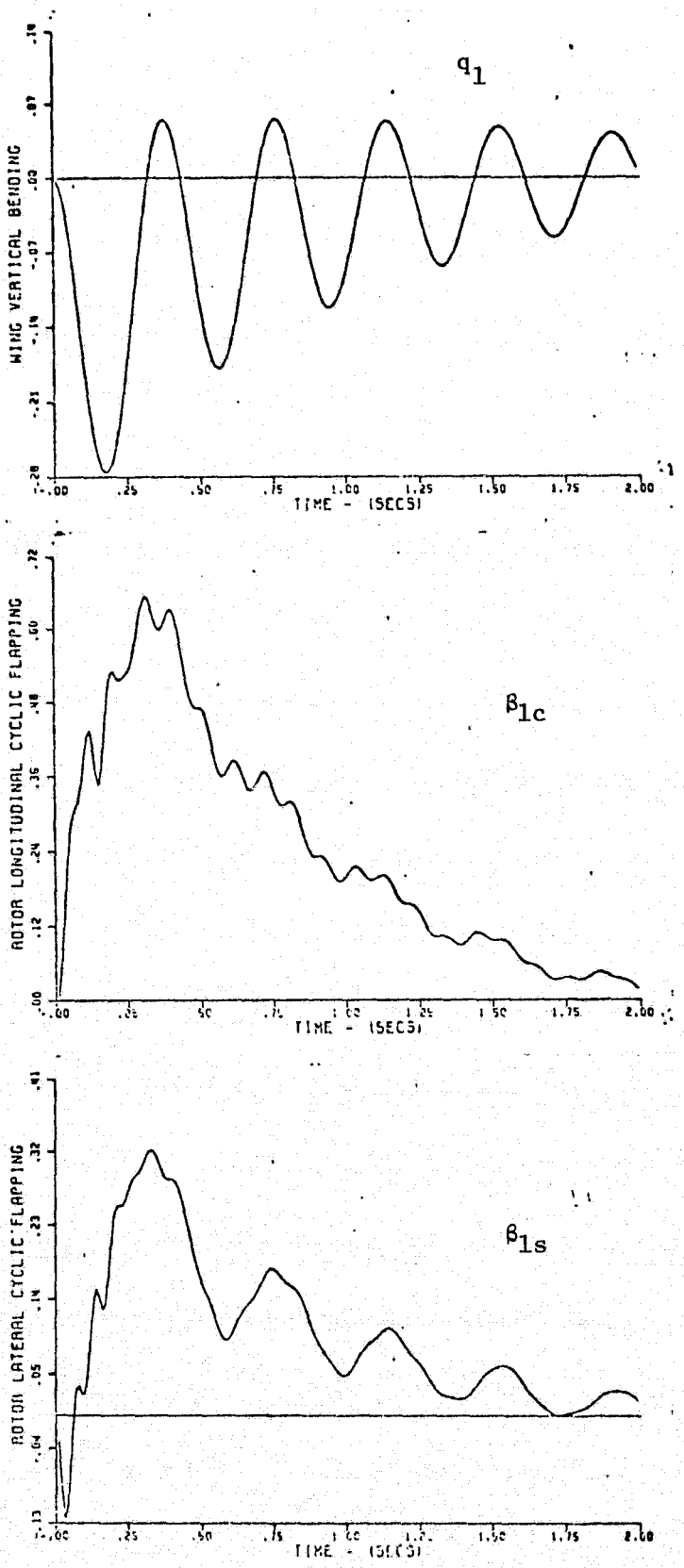

Figure II-4. Uncontrolled Airplane Response to a Shaped Pulse of Vertical Gust Velocity.

the forward speed. Similarly the rotor flapping responses are 0.590 (radian/radian)(longitudinal) and 0.253 (radian/radian)(lateral). Using these data, 1.0 ft/sec (RMS) vertical gust velocity results in 0.08 inch (2.1 mm) (RMS) deflection of the wing tip and 1.4 milliradians (RMS) of longitudinal flapping. Under heavy turbulence with 20 ft/sec (RMS) vertical gust velocity, these become 4 cm tip deflection and 28 mr., or 1.6 degree, of flapping.

The mathematical model for the wing-rotor assemblage considers that structural damping is very low. The experimental measurements made using the wind tunnel model indicate that damping ratios of the various modes are typically higher by a factor of 4 over those predicted by the analytical representation. Whether or not this same difference will carry over to the full scale airplane is not known, but allowance for uncertainty in knowledge of mode characteristics should be included in studies of contemplated active control systems.

The model also assumes an autorotating rotor. This is the case for the wind tunnel model. When the rotor rotational degree of freedom is modelled for the powered flight case, it is found that the changes to the system transfer functions including this added response mode are less than 1%. Thus the control system design will not be changed significantly, and the simpler representation omitting this mode can be used.

Chapter III

CONTROL SYSTEM SYNTHESIS

Following the synthesis approach outlined in Chapter I, attention was directed first to simple single feedback control system configurations. The performance limitations of such systems were assessed, and then the capability of multiple feedback paths and the use of multiple control effectors for extending the performance were examined. The performance criterion was taken to be the root mean square response that results while flying through random atmospheric turbulence. The mean square value of a random variable is given as the integral with respect to frequency of its power spectral density. This in turn is a function of the square of the magnitude of the frequency response of the closed-loop system. The transfer functions of interest here relate the wing vertical bending coordinate and the rotor blade flapping to an atmospheric gust input.

Figure III-1 presents the general functional block diagram for the single feedback control system. In such a control loop the servo needed to drive the control effector is an element in the feedback path, and as such its poles appear as closed loop zeroes. Any servo lags will correspondingly increase the (RMS) value over that obtained with an ideal servo, since the zeroes will increase the magnitude of the frequency response. Thus one is driven in the direction of asking for servo bandwidth that is high relative to the bandwidth of the gust input and of the response modes that dominate the response. To obtain a preliminary estimate of the capability of an active control system for reducing bending and flapping, the initial studies assumed ideal, or no dynamic lag, servo characteristics. The effects of the servo are then discussed in Chapter IV.

Quantitative Gain Values

Insight for interpreting the numerical gain values that are listed in the results of these analyses is provided in the following way. The design parameter that is of prime significance in establishing the performance

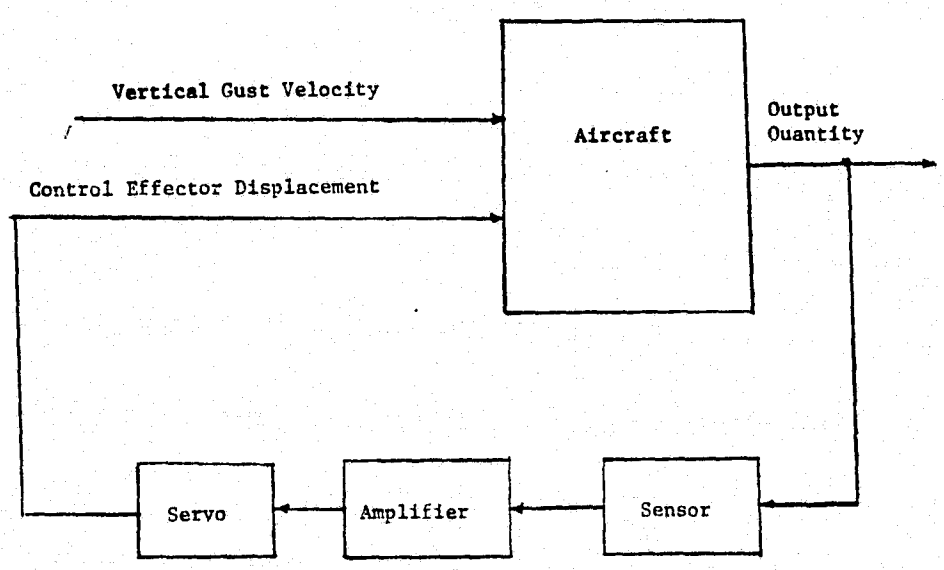

Figure III-1. General Functional Block Diagram, Single Feedback Control System.

capability of these closed loop control systems is the open loop static sensitivity, S_{OL}, where

$$S_{OL} = S_{cs[x,\delta]} \, S_{A[\delta,x]}$$

and

$S_{cs[x,\delta]}$ = the static sensitivity of the control system feedback path relating the incremental change in the control effector, δ, to an incremental change in measured output quantity, x, in static or steady state conditions

$S_{A[\delta,x]}$ = the static sensitivity of the airplane relating the incremental change in the output quantity, x, produced by an incremental change in the control effector, δ, in static conditions.

At a given flight condition the airplane's static sensitivity is unalterable, and hence the designer only has freedom to vary the control system static sensitivity, $S_{cs[x,\delta]}$. Results are accordingly expressed in terms of S_{cs} rather than S_{OL}, and the airplane static sensitivities can be obtained from the data in Appendix A. Since no summing point has been shown on the block diagram of Figure III-1, the algebraic sign of the complete feedback path is included with the numerical data. If S_A is positive, the usual negative feedback case then requires S_{cs} to be negative.

To establish a basis for the quantitative gain data, it is helpful to consider the change in control effector displacement produced by a unit change in a measured output quantity when the control system static sensitivity is unity. The wing vertical bending coordinate, q_1, is the bending displacement nondimensionalized by the wing semispan, which is 200 inches. Thus for a 1 inch bending deflection (at the wing tip) and a control system static sensitivity of 1.0, the control effector displacement would be (1/200) radian, or 5 milliradians, or 0.3 degrees. If for example the control system authority were 10 degrees, a control system static sensitivity of unity would call for 3 per cent of the available control travel for a 1 inch bending displacement. Thus one can ratio these results for other

assumed values of control authority and output displacements to establish the percentage of full travel that is being commanded by the control system. As an example, if the bending to wing flap static sensitivity were 18, a one inch deflection of the wing tip would produce 5.4 degrees of flap deflection. If the control authority were 10 degrees of flap, this represents 54 per cent of full travel per inch of deflection.

Control System Designation

In the sections that follow, the various feedback configurations are designated by system numbers as follows:

System 1-i: ith single feedback, single control effector system
System 2-i: ith multiple feedback, single control effector system
System 3-i: ith multiple feedback, multiple control effector system.

1. Single Feedback Loop Configurations

Considerable insight into the effect of various feedback configuration possibilities can be obtained from examining single loop systems using the various easily measured output quantities one at a time fed to the several control effector choices. The contribution of the individual path in more complicated configurations is then easier to interpret.

System 1-1. Wing vertical bending, q_1, fed to the rotor blade longitudinal cyclic control, θ_{1s}:

Since rotor blade longitudinal cyclic control produces vertical forces, it is natural to investigate the use of this control for reducing bending. Figure III-2 presents a mathematical block diagram for an idealized control system which feeds q_1 to θ_{1s}. Using this feedback path the (RMS) values of both the wing vertical bending and the rotor flapping can be reduced. Figure III-3 presents the root locus for this system. The parameter that is varied along the root loci is the open loop static sensitivity, S_{OL}, given by

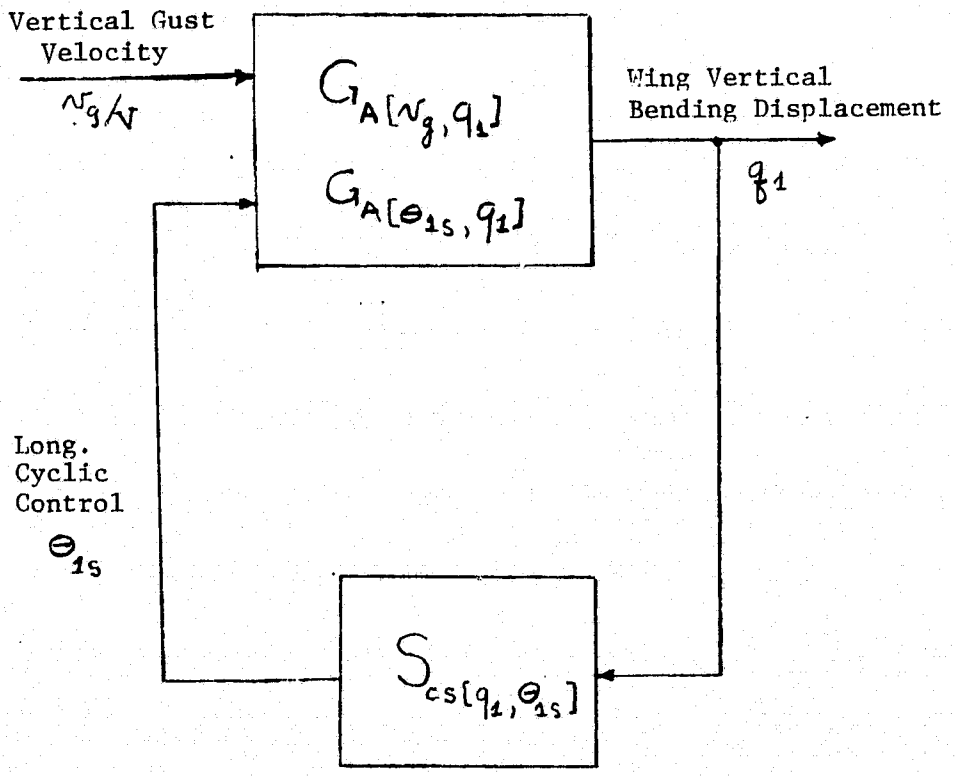

Figure III-2. System 1-1. Mathematical Block Diagram.

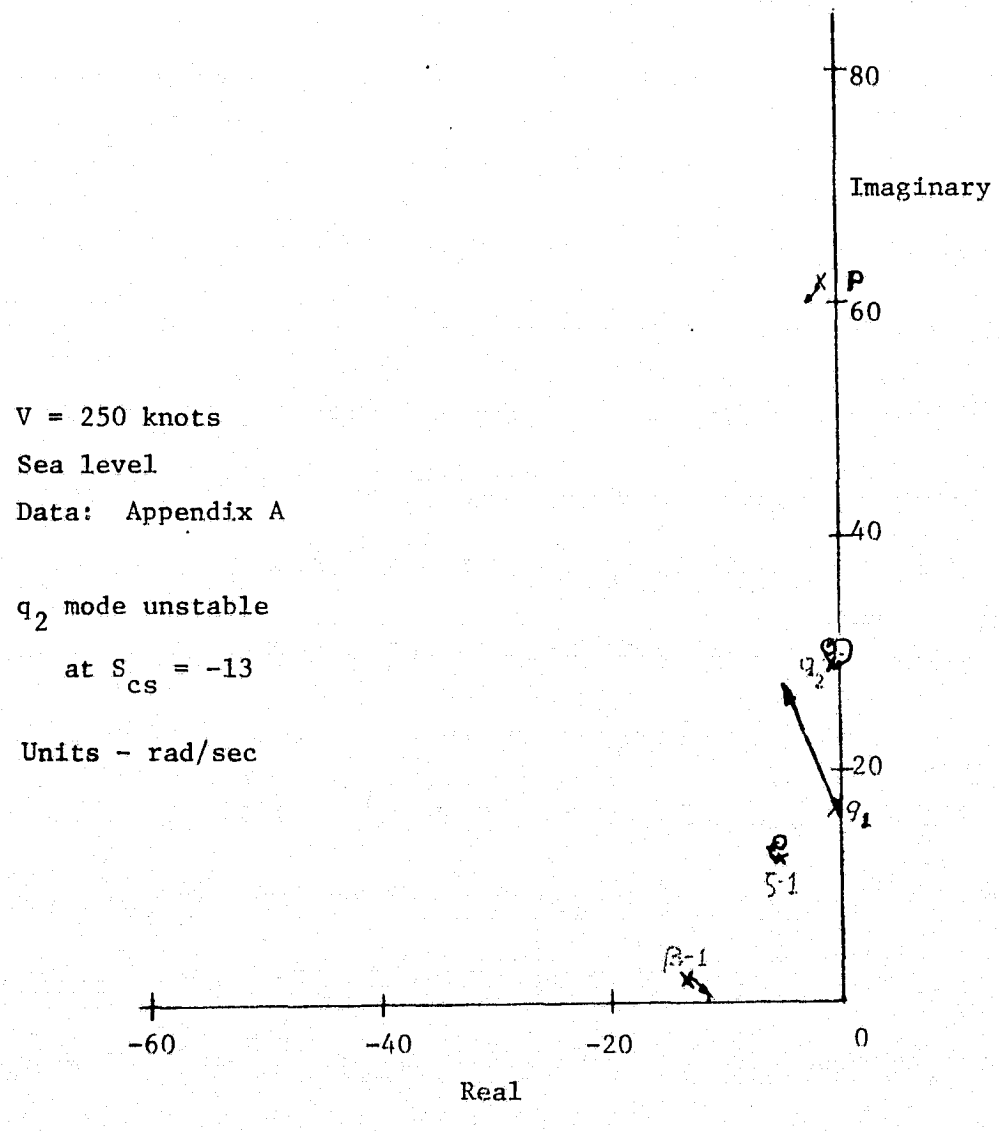

Figure III-3. Root Locus. System 1-1. Wing Vertical Bending Displacement Feedback to Rotor Blade Longitudinal Cyclic Control.

$$S_{OL} = S_{A[\theta_{1s}, q_1]} \; S_{cs[q_1, \theta_{1s}]}$$

where

$S_{A[\theta_{1s}, q_1]}$ = static sensitivity of the airplane relating the wing vertical bending coordinate, q_1, to the rotor longitudinal cyclic control deflection, θ_{1s}, in steady state.

$S_{cs[q_1, \theta_{1s}]}$ = static sensitivity of the feedback path of the control system relating the rotor longitudinal cyclic control deflection, θ_{1s}, to the measured wing vertical bending coordinate, q_1, in steady state.

At a given flight condition the airplane's static sensitivity is constant, and hence it is convenient to express changes in S_{OL} as changes in the feedback path static sensitivity. As the open-loop static sensitivity is increased, the effective static stiffness of the wing is increased as shown by the increased natural frequency of the wing vertical bending mode, q_1. In addition the exponential factor of the mode (the real part of its eigenvalue) increases causing oscillations to decay faster. If it were practical to increase the gain without limit, and if there were no other response modes, one would use very large values of S_{OL}. However, at this flight condition as S_{OL} is increased, Figure III-3 shows that the wing chordwise mode becomes unstable at a value of control system feedback path static sensitivity of approximately -13.

Figure III-4 presents a summary of the reduction in (RMS)q_1 that results with this feedback configuration. It indicates that the minimum bending response is obtained at a feedback gain of approximately -12 and represents a 51 per cent reduction of the response of the uncontrolled airplane (RMS ratio of 0.49). Plotted on the same figure also is the reduction in (RMS) levels of rotor flapping, β_{1s} and β_{1c}. The reduction in flapping occurs because the longitudinal cyclic angle change produced by the feedback loop counteracts the flapping caused by the gust input. The gust spectrum is essentially low frequency relative to the rotor flapping and bending response modes. Over this frequency range the rotor flapping and the wing

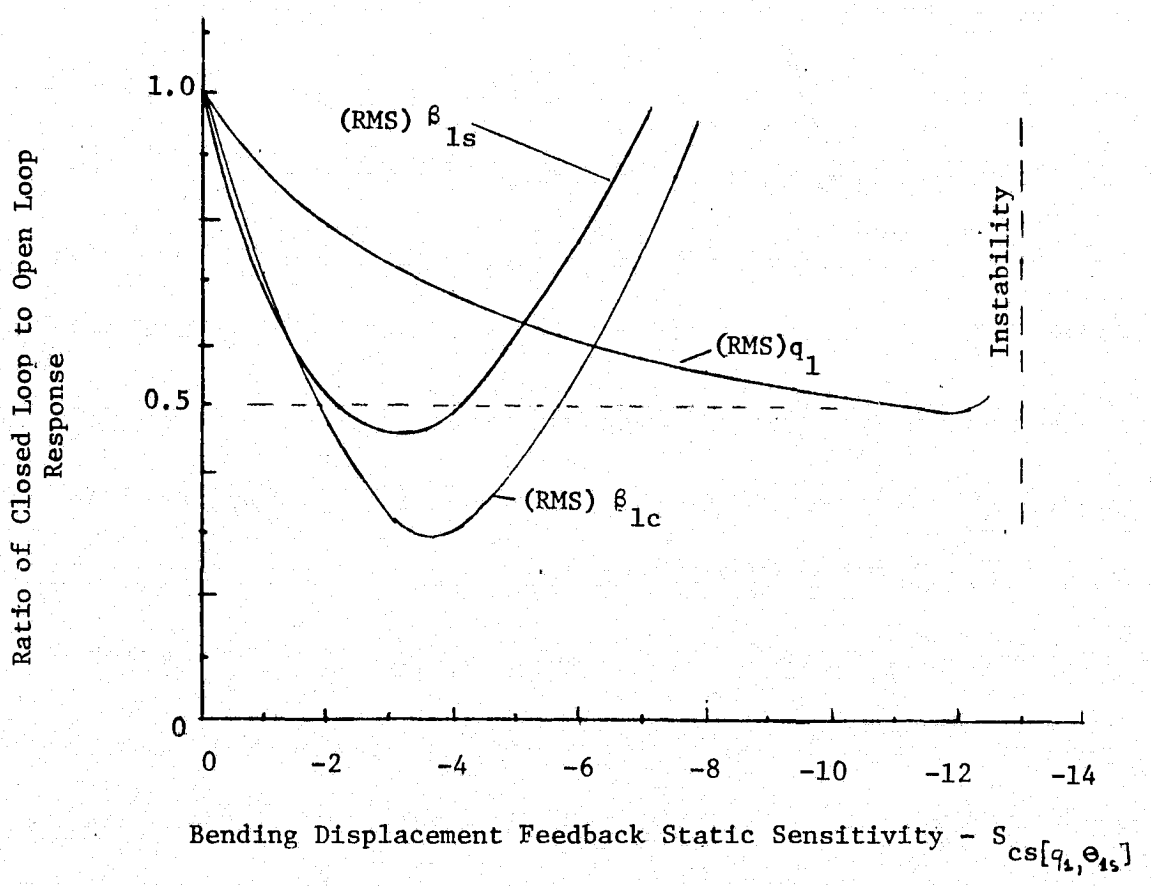

Figure III-4. System 1-1. Variation with Control System Feedback Static Sensitivity of the Ratio of the (RMS) Levels of Closed Loop Control System Response to Uncontrolled Airplane Response.

bending displacement are nearly in phase with the gust input. An upward gust causes the top of the rotor plane to tip aft and the wing tip to displace upward. For an upward bending displacement, the feedback path causes a longitudinal cyclic change that tips the rotor plane forward, thereby reducing the flapping motion. As the feedback gain is increased however, the longitudinal cyclic change produced by the control system becomes greater than that needed to offset the flapping due to the gust input. Thus a minimum point is reached in the plot of the (RMS) value of flapping versus control loop static sensitivity, and Figure III-4 shows that this occurs at a lower value of gain than does the minimum point for the bending motion. The figure shows however that the fractional reduction in flapping is lower than that of bending, and one could use feedback static sensitivities as high as -8.0 before amplifying the flapping above that level which the uncontrolled airplane would exhibit. If one were to use the still higher value of -12 corresponding to approximately the maximum value that could be used to reduce bending displacement, the longitudinal cyclic flapping would be amplified by a factor of 1.6 and the lateral cyclic flapping by a factor of 1.7 over the uncontrolled airplane response.

The use of this feedback configuration changes the nature of the flapping motion however. The transient time response of bending and flapping motions shows this. As introduced in Chapter II, Figure II-3 presented a pulse input obtained by feeding a unit impulse to a filter that has the bandwidth characteristics of the spectrum of the gust input model. Such a pulse response tends to excite the system modes that dominate the response during the turbulence input. With the control feedback configuration of Figure III-2, the shaped pulse gust input produced the responses shown in Figure III-5. A feedback gain of -4.05 was used which is above the minimum flapping point, so that the flapping response to the gust has been overcompensated in favor of reducing the bending response. This gain value provided a gain margin of 3, and the (RMS) level of bending was reduced by 32%. Comparing Figure III-5 with Figure II-4 for the uncontrolled airplane, it is evident that one effect of the control system is that a large component of the wing bending mode now shows up in the

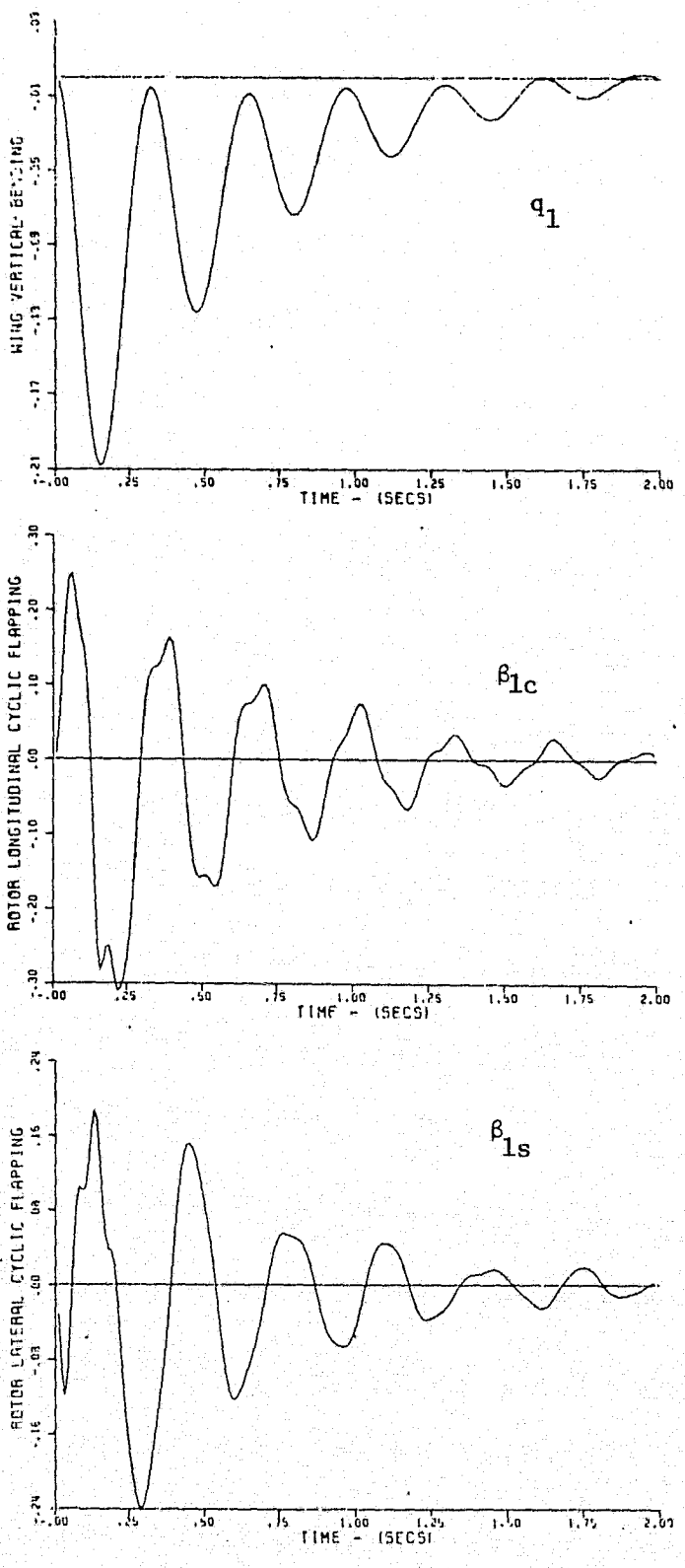

Figure III-5. System 1-1. Response to Shaped Pulse of Vertical Gust Velocity. $S_{cs} = -4.05$.

flapping motion. Compared with Figure II-4, the reduction in bending evident in Figure III-5 is not very dramatic for this input, although the increased damping and stiffness can be observed. Note that in these computer generated plots, the ordinate scales were changed, and the peak value of the bending is less in Figure III-5 than in Figure II-4.

The increased flapping motions at the bending mode frequency may be objectionable and may result in an operational requirement for much higher damping of the bending mode if this feedback configuration were to be used. In any event when selecting a control system feedback sensitivity on the basis of Figure III-4, assuming no other constraints were present, there must be a stated tradeoff between reducing the be nding and reducing the flapping.

The analysis predicted that the improvement in bending response would continue as the open loop static sensitivity was increased. Due to the presence of the zeroes near the poles of the chordwise bending mode (see Figure III-3), there is little excitation of the chordwise bending and hence little contribution of that mode to the (RMS) values shown in Figure III-4. However as the stability limit is approached, this mode becomes more noticeable, and the curves of the (RMS) responses would rise very steeply as the limiting value of gain was approached. The critical gain value is sensitive to the damping ratio of the chordwise bending mode. Figure III-6 presents a plot of critical value of S_{OL} versus $(\zeta\omega_n)$ of the chordwise bending mode, for changing $(\zeta\omega_n)$ by a factor of 2 in each direction from the predicted value. If $(\zeta\omega_n)$ were decreased, Figure III-6 shows that the critical open-loop gain decreases rapidly. Although not shown in Figure III-3, the effect of increasing $(\zeta\omega_n)$ upon the root locus would be to cause the locus branch emanating from the chordwise bending mode to depart toward the left and then turn upward, while the branch originating at the wing bending mode becomes less damped, enters the right half plane near the chordwise bending mode, and proceeds to the zero. Thus there is an unstable closed-loop mode in the region of the open-loop chirdwise bending mode at high loop gain even for increased $(\zeta\omega_n)$. At low values

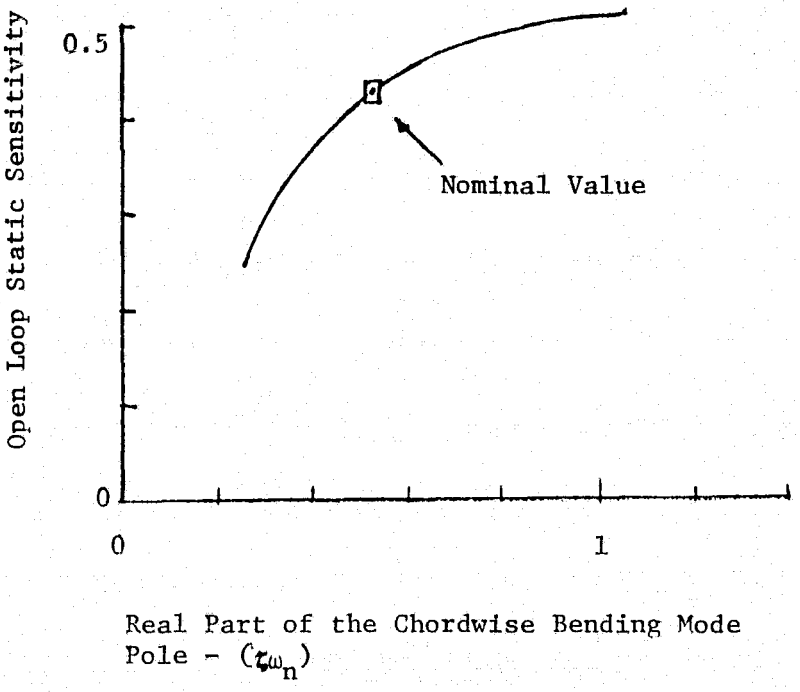

Figure III-6. Variation of the Critical Open Loop Static Sensitivity with the Real Part of the Chordwise Bending Mode Pole.

of loop gain, approximately the same behavior of the vertical bending mode response would be expected with any of the locations of the chordwise bending mode, but the uncertainty in gain margin is something that needs to be accounted for. Indeed one would want to compensate the system if possible to increase gain margin and thereby decrease the sensitivity to uncertainty of the modelling of the plant.

It is to be further noted that Figure III-3 predicts that the chordwise bending becomes stable again at a higher value of loop gain as the root locus branch closes to the nearby zero. Hence a mathematically optimum

feedback gain would be higher than that used above resulting in a theoretically lower minimum bending value. Such a conditionally stable control system has been discounted here as being poor design practice for a safety of flight application of this type. Other optimization procedures may lead to similarly conditionally stable system design, and high gain configurations should be checked in this regard.

System 1-2. Wing vertical bending velocity, $\dot{q}_1$, fed to the longitudinal cyclic, θ_{1s}:

It is natural to consider the use of the rate of change of the bending coordinate as a feedback signal. The configuration of Figure III-2 would apply if the feedback quantity is changed to $\dot{q}_1$. Figure III-7 presents a root locus plot for this single feedback configuration. The feedback directly improves the damping ratio of the wing vertical bending mode to the moderate extent that that branch of the locus approaches the zero located near the low frequency blade lagging mode. This increased damping decreases the time for the bending motion to decay in response to a disturbance and also decreases the peak response. There is a corresponding reduction in the (RMS) level of the bending motion. Figure III-8 summarizes the reduction in (RMS) motion using only bending rate feedback to the longitudinal cyclic control. The reduction in (RMS) bending is less than was achieved with system 1-1 since this feedback does not result in an effective increase in bending stiffness.

The root locus for this single feedback system shows that the critical mode is the wing torsion mode. The damping of the wing chordwise bending also decreases, but for the data used, that mode remains stable. The bending mode poles approach the zeroes located near the lagging mode. The poles of the latter decrease in frequency without much improvement in damping ratio. For an open loop gain at the boundary of stability, the bending mode exhibits a damping ratio of 0.3 and the lagging mode a damping ratio of 0.4. Thus if an adequate stability margin were to be provided, less damping would have to be accepted unless additional com-

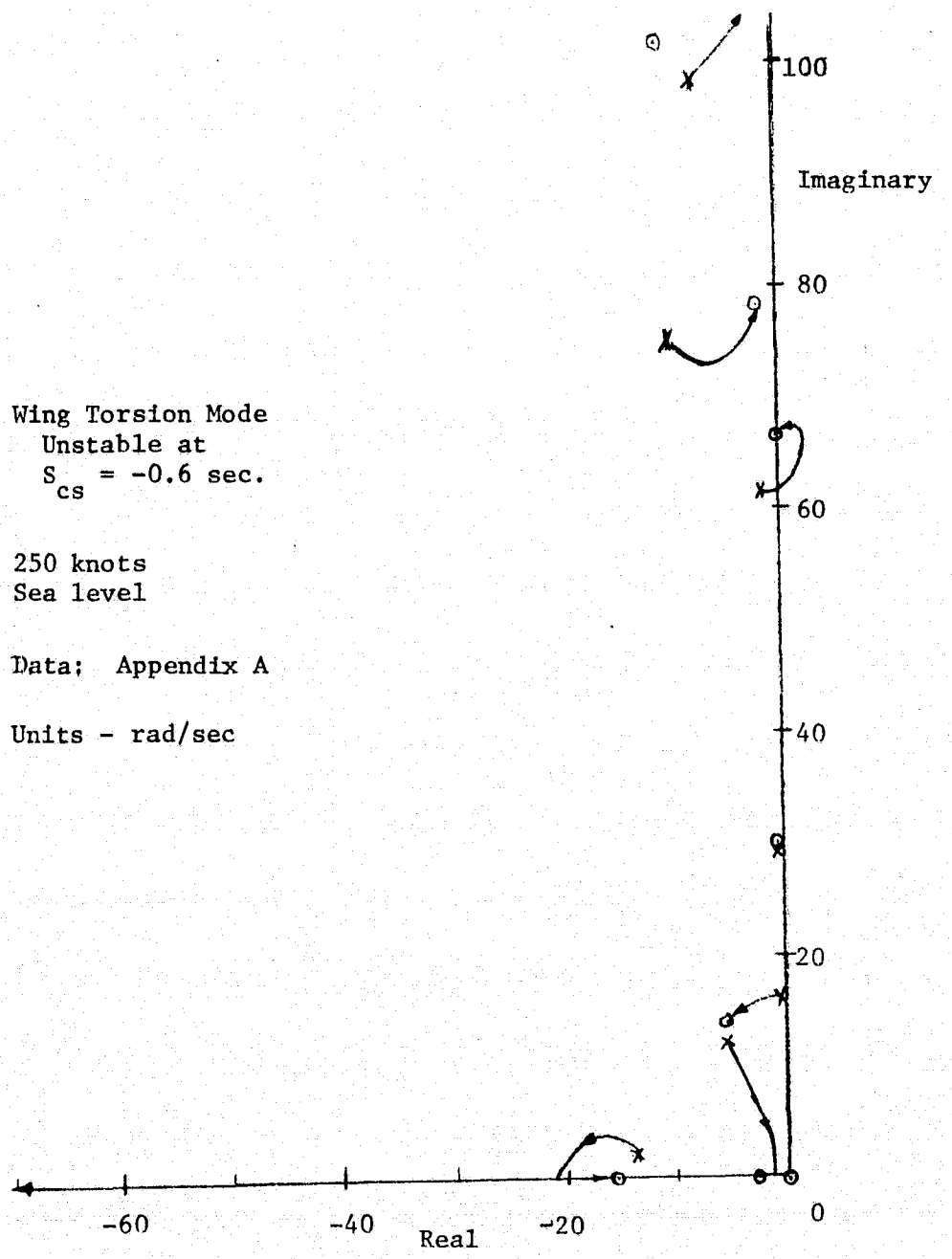

Figure III-7. Root Locus. System 1-2. Wing Vertical Bending Velocity Feedback to Rotor Blade Longitudinal Cyclic Control.

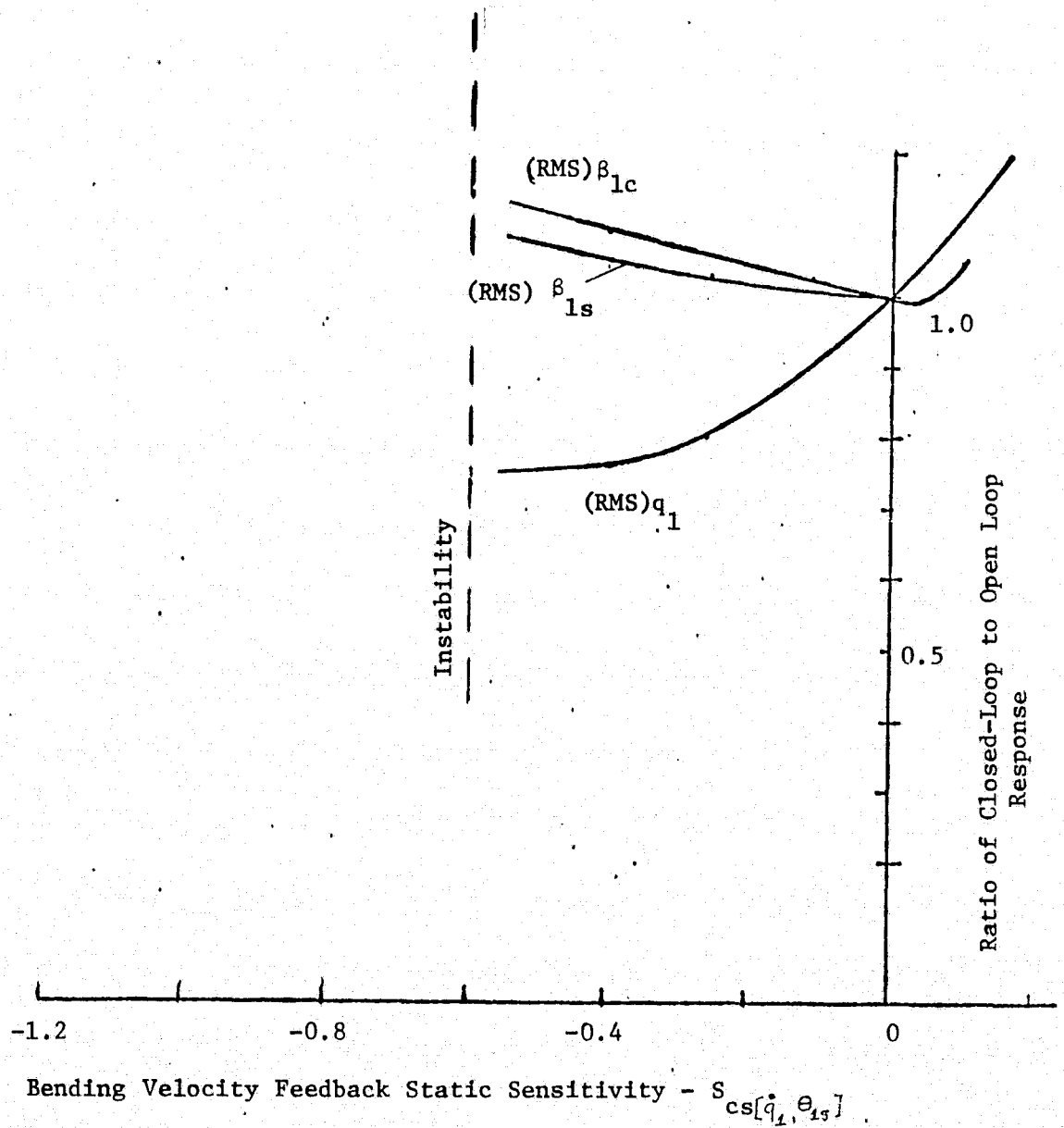

Figure III-8. System 1-2. Variation of the Ratio of (RMS) Level of Closed Loop Control System Response to Uncontrolled Airplane Response with Control System Feedback Static Sensitivity.

pensation could be provided in some form. For a stability gain margin of 4, the damping of the bending mode is only 0.15, although this is significantly better than the 0.04 value of the uncontrolled airplane. The transient pulse response using this gain is shown in Figure III-9. The torsion mode excitation is very evident in the longitudinal flapping pulse response. The coupling with the wing torsion mode thus limits the effectiveness of the bending rate feedback configuration. This has been found to be a characteristic feature of this feedback path, and when one examines the performance of multiple feedback paths, the use of wing vertical bending rate feedback to the rotor longitudinal cyclic provides a relatively small incremental improvement in performance in terms of the (RMS) level of bending to be expected in turbulence.

Since the bending velocity is 90 degrees out of phase with the flapping motion at low frequency, the use of $\dot{q}_1$ fed to θ_{1s} does not reduce the low frequency flapping. Indeed the flapping motion needed to increase the bending mode damping results in an amplification of the (RMS) flapping as shown in Figure III-8. The pulse response of flapping, shown in Figure III-9, indicates that the low frequency response is somewhat greater compared with the response of Figure II-4. Compared with system 1-1, the bending response has greater damping, and there is a smaller component due to the bending mode in the flapping response. The previously stated caution about the inaccuracy in knowledge of these modes applies with this configuration as with that of system 1-1.

System 1-3. Wing vertical bending, q_1, fed to lateral cyclic θ_{1c}:

Although it is difficult to find a physical motivation for using rotor blade lateral cyclic control for controlling wing bending, it is included for completeness. This control does excite wing bending to an extent approximately comparable to that produced by longitudinal cyclic, but the transfer function relating bending to the lateral cyclic exhibits a right half plane zero at 24 (rad/sec) which is detrimental to the use of this control. The root loci of Figure III-10 shows that q_1 feedback

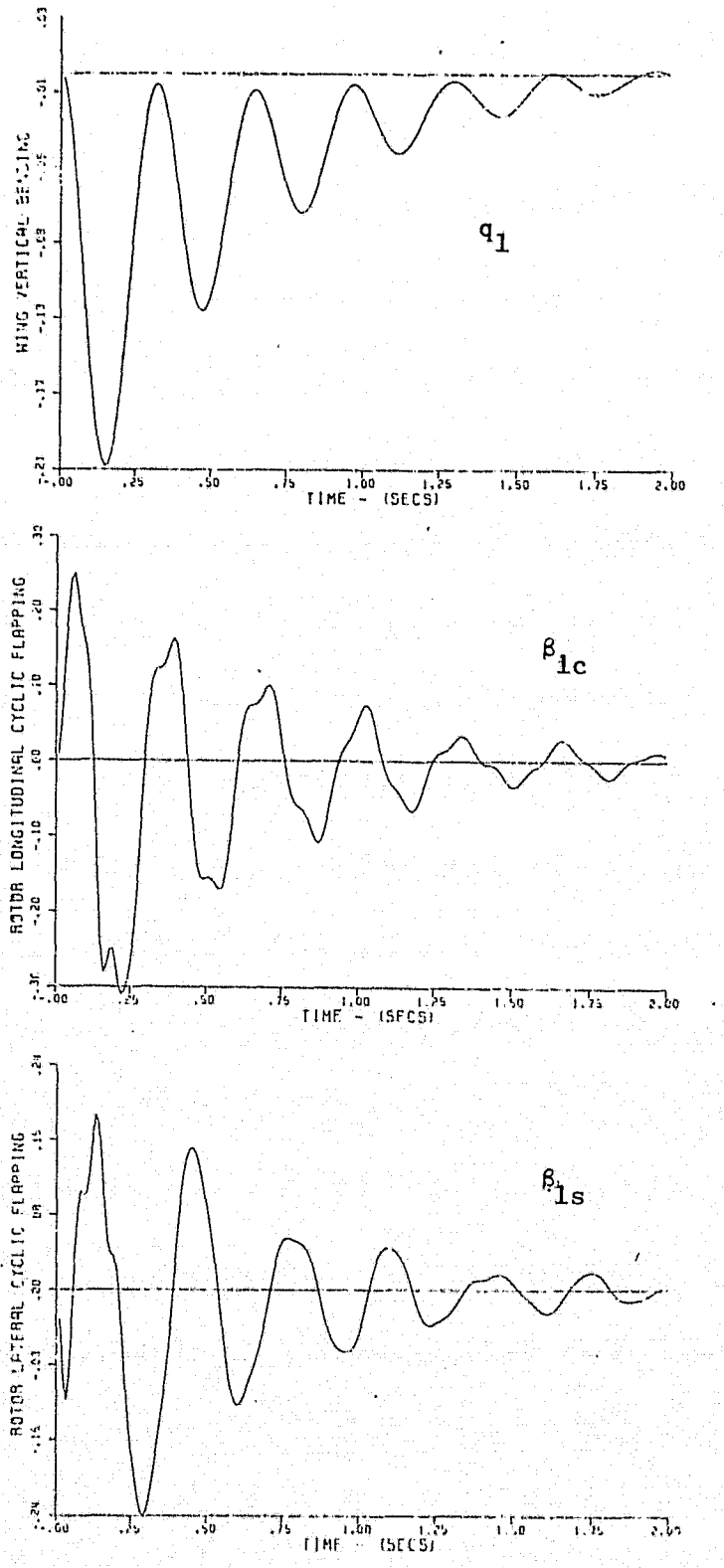

Figure III-9. System 1-2. Response to a Shaped Pulse of Vertical Gust Velocity. S_{cs} = -0.15 sec.

destabilizes the wing vertical bending mode, while $\dot{q}_1$ feedback destabilizes the chordwise bending mode. These plots assume a positive open loop static sensitivity. Using a negative S_{OL} reverses the order of mode instabilities, but does not change the overall conclusion that this is an unacceptable control configuration.

Although it is unlikely that one would use the rotor lateral cyclic control alone to change the characteristics of wing bending, the combined use of θ_{1s} and θ_{1c} is equivalent to rotating the azimuth reference for the rotor cyclic blade angle change. Hence the effect of this feedback path is of interest. Discussion of the use of both cyclic controls more properly belongs in the section on multiple controllers of this report, but it will be included here from the standpoint that the combination is equivalent to a single feedback at a different azimuth reference. It was found that optimizing the feedback sensitivities to the two cyclic controls to reduce bending or flapping motions verified that feeding the bending information to the lateral cyclic is ineffective. Therefore one would want to use only the rotor blade longitudinal cyclic control for this purpose.

System 1-4. Wing vertical bending, q_1, fed to a trailing edge wing flap, δ_f:

One could expect to obtain a direct change in wing life through actuation of a trailing edge flap, and hence one would expect this control to be effective in controlling wing vertical bending. A possible candidate surface for this use would be flaperons used both as flaps and as ailerons. Reference 2 suggested a possible flap design which had a 30% chord and 50% span dimension. This has been used in these studies. However it is probably too large and sensitive for use in controlling bending. For safety of flight reasons, one would no doubt wish to use smaller and perhaps redundant surfaces for this application. Thus the results described here should be considered as showing trends, and gain values would have to be scaled accordingly for other desired span or chord dimensions.

The root locus for this single feedback controller is presented in

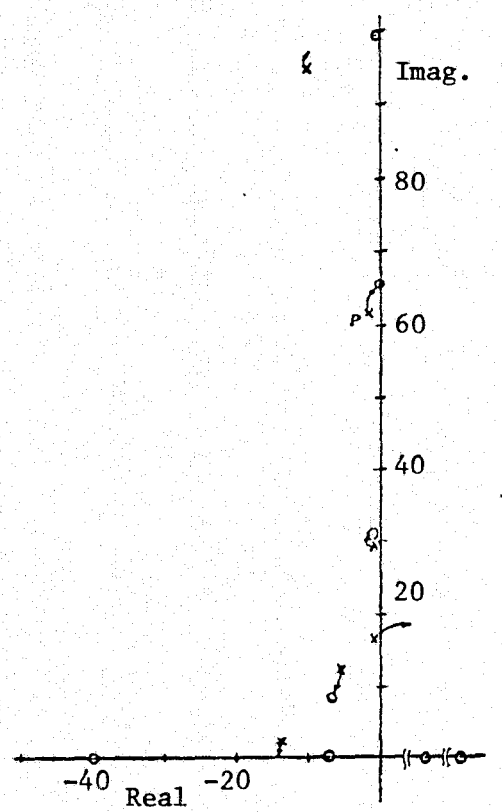

(a) Vertical Bending Displacement Feedback

Units - rad/sec

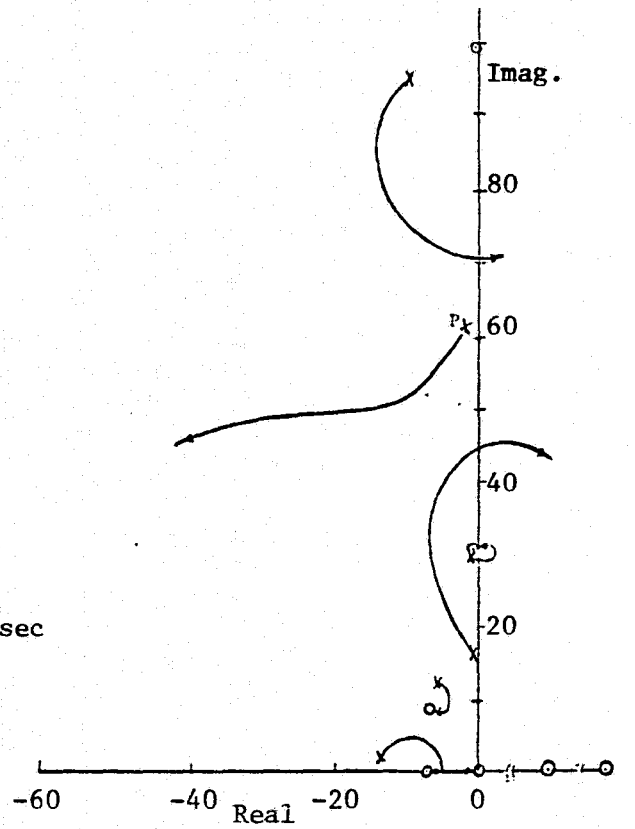

(b) Vertical Bending Velocity Feedback

Figure III-10. Root Locus. System 1-3. Wing Vertical Bending Feedback to Rotor Blade Lateral Cyclic Control.

Figure III-11. Primarily it is the bending mode that is excited by the flap as evidenced by the pole zero cancellation of other modes. The effect of this feedback is to increase the effective bending stiffness with no improvement in damping ratio. Figure III-12 summarizes the effects of the control system upon the (RMS) responses of bending and flapping in turbulence. Improved bending response is obtained with little change in flapping. In analogy to the discussion of system 1-1, one would expect to see appreciable flap motion at the bending mode frequency due to this feedback, since the damping ratio of the bending mode remains low.

System 1-5. Wing vertical bending rate, $\dot{q}_1$, fed to a trailing edge flap δ_f:

If bending rate is fed to the flap, there is a direct improvement in damping ratio of the bending mode as shown by the root locus of Figure III-13. This improved damping results in reduced bending as shown by Figure III-14. Little change in flapping results. The large reduction in bending for low values of feedback gain is indicative of the sensitivity of this large flap.

System 1-6. Rotor cyclic flapping coordinate, β_{1c}, fed to rotor longitudinal cyclic, θ_{1s}:

Since it may be possible to provide instrumentation that would measure the rotor blade flapping, one might be interested in using that signal to form a feedback configuration for the purposes of controlling flapping. Root loci for this feedback are shown in Figure III-15. There is little change in the pole locations for open loop static sensitivities that give stable operation. The critical mode is predicted to be the wing torsion mode which becomes unstable at a feedback gain of 0.65. There is a reduction in (RMS) flapping due to the effect of the feedback in reducing closed-loop static sensitivity, as shown in Figure III-16. Little change in bending results.

The use of rate of change of longitudinal flapping also provides

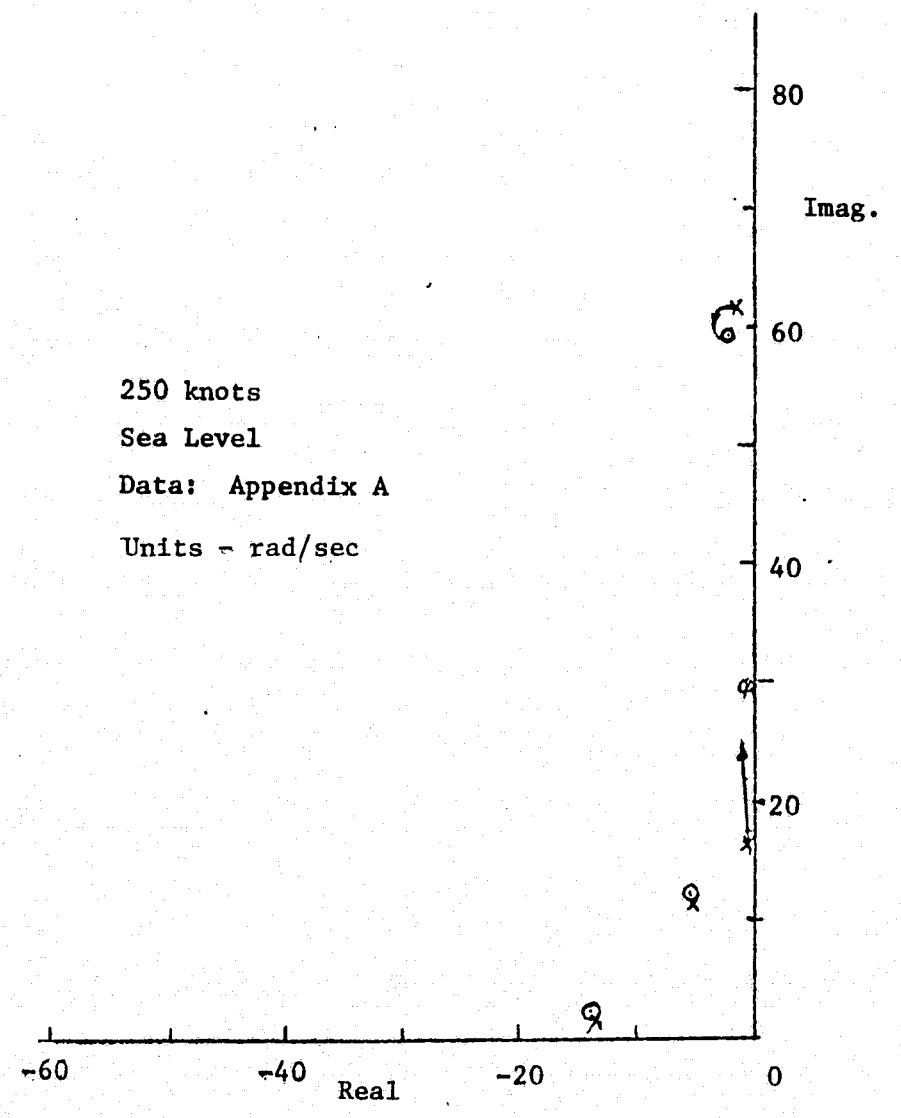

Figure III-11. Root Locus. System 1-4. Wing Vertical Bending Displacement Feedback to Wing Flap.

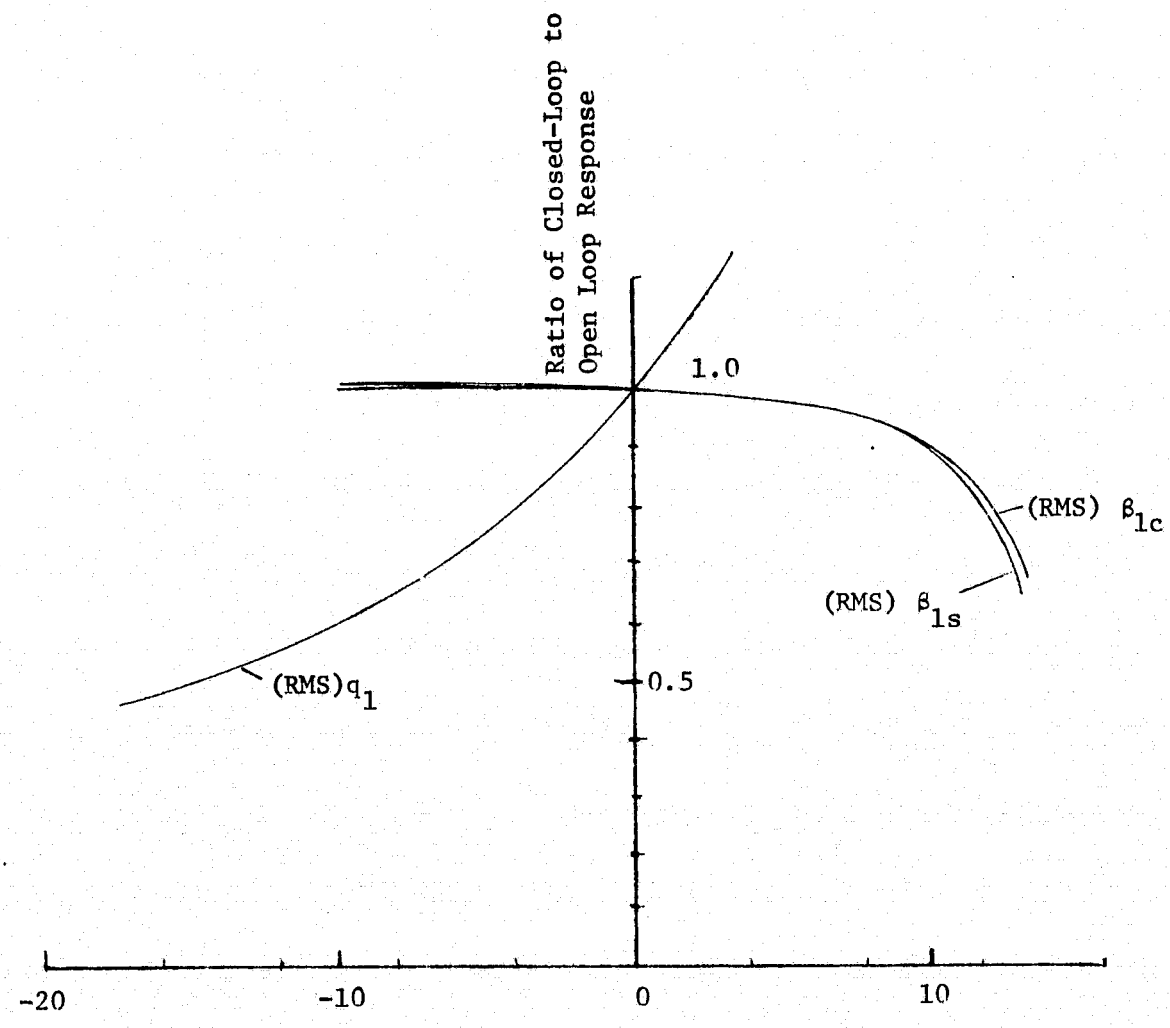

Figure III-12. System 1-4. Variation of the Ratio of (RMS) Level of Closed Loop Control System Response to Uncontrolled Airplane Response with Control System Feedback Static Sensitivity.

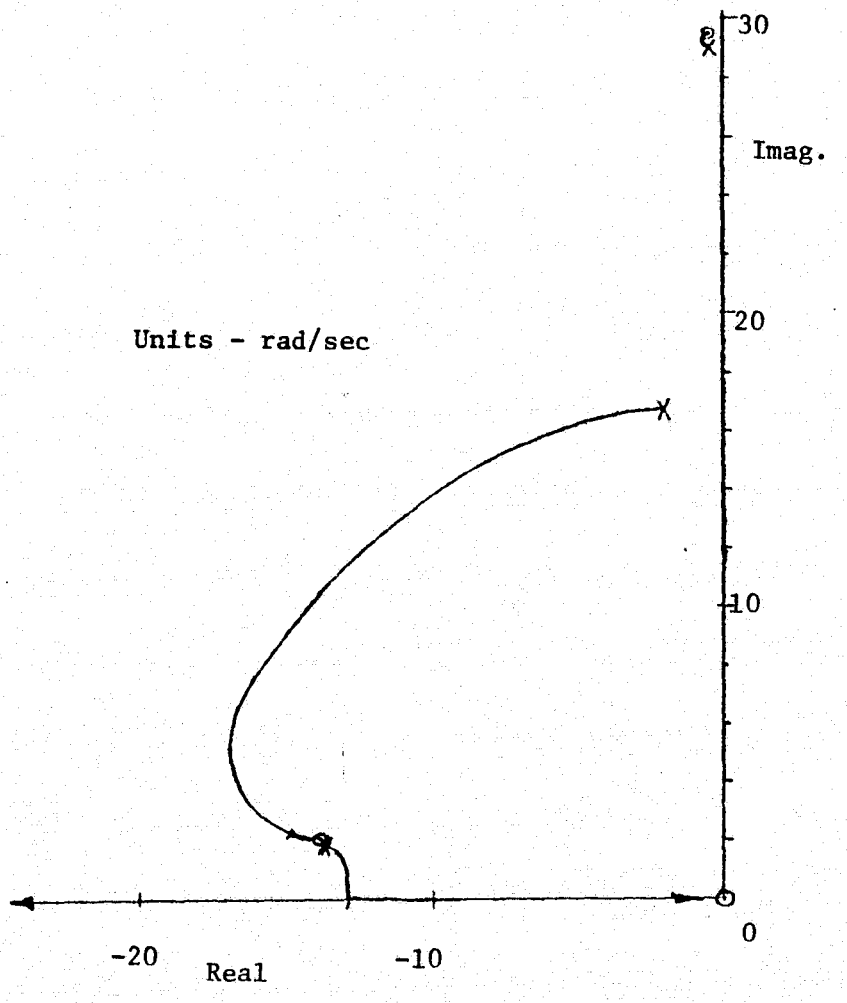

Figure III-13. Root Locus. System 1-5. Wing Vertical Bending Velocity Feedback to Wing Flap.

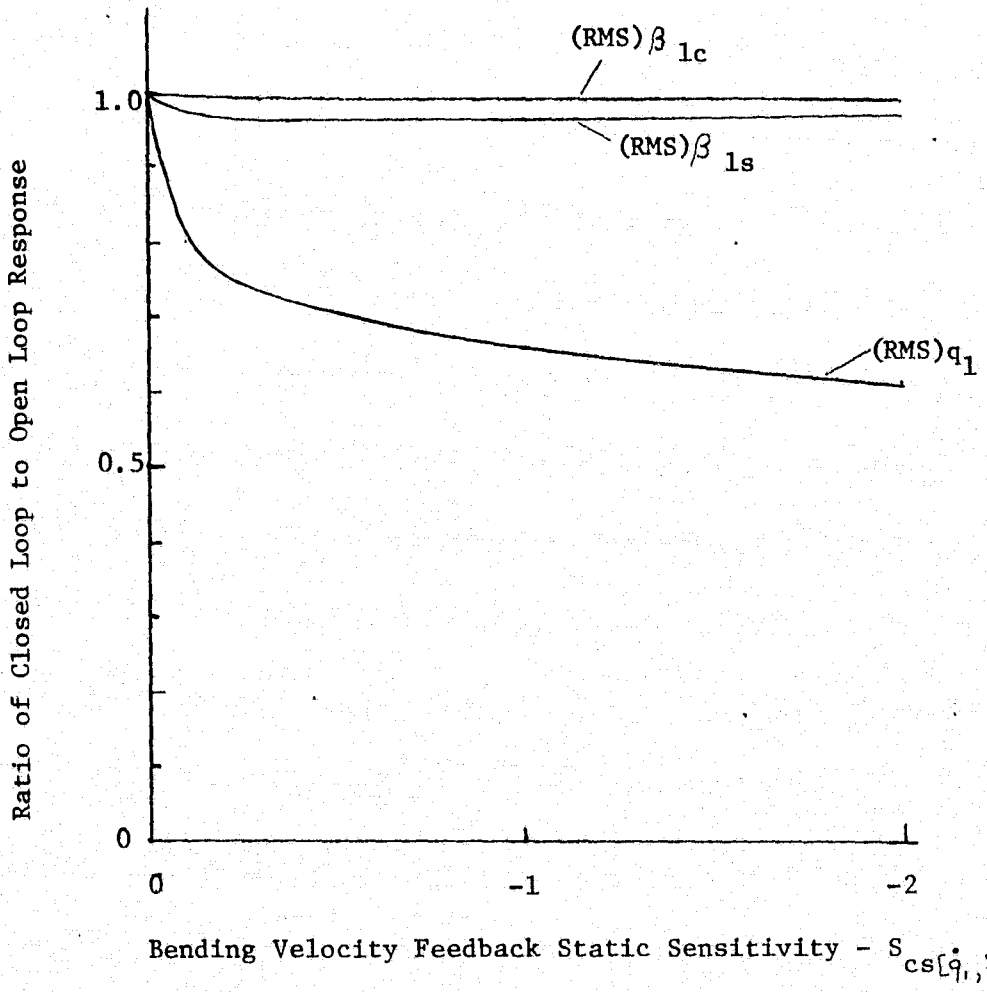

Figure III-14. System 1-5. Variation with Control System Feedback Static Sensitivity of the Ratio of the (RMS) Levels of Closed Loop System Response to Uncontrolled Airplane Response.

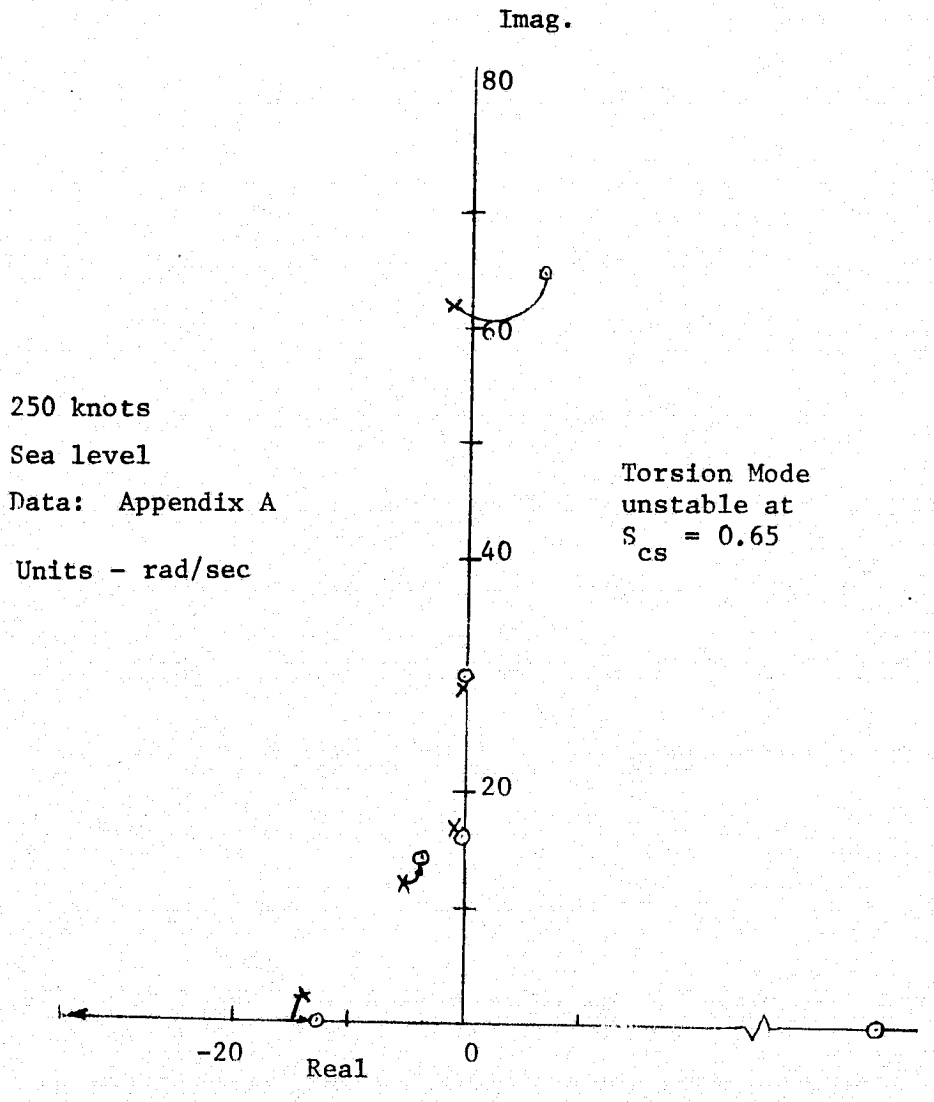

Figure III-15. Root Locus. System 1-6. Rotor Blade Longitudinal Cyclic Flapping Displacement Feedback to Rotor Blade Longitudinal Cyclic Control.

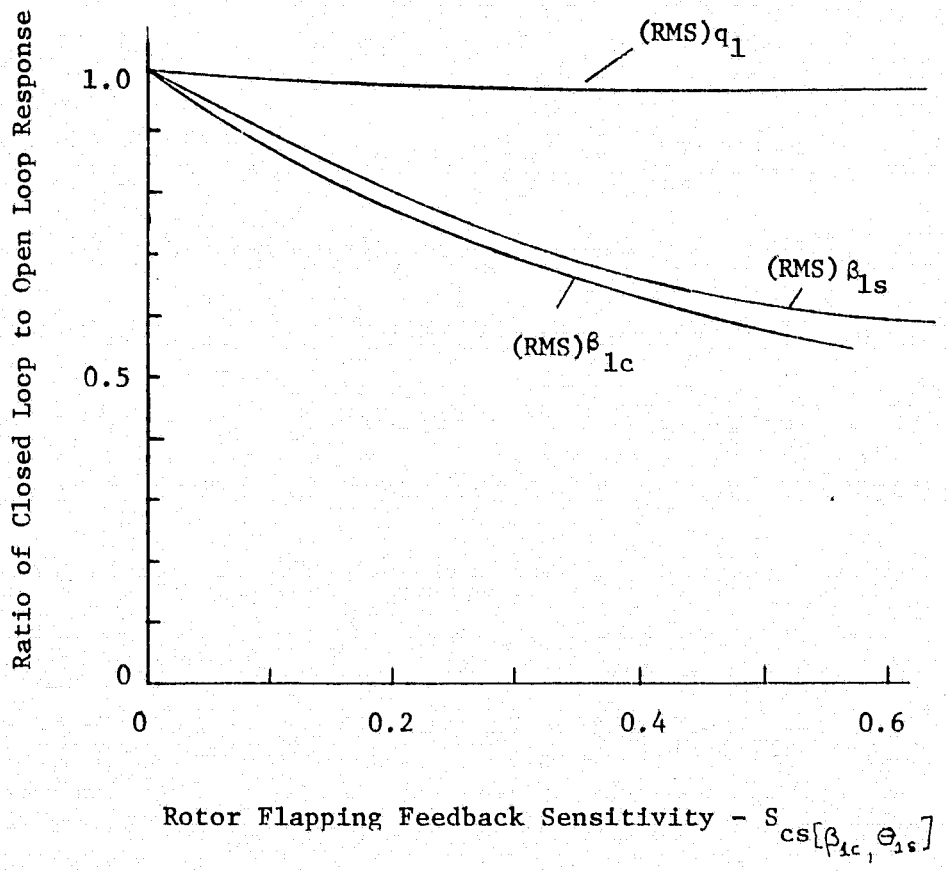

Figure III-16. System 1-6. Variation with Control System Feedback Static Sensitivity of the Ratio of the (RMS) Levels of Closed Loop System Response to Uncontrolled Airplane Response.

little change in dynamic characteristics and has no effect upon static response. Thus it is of little utility as a candidate feedback configuration.

System 1-7. Rotor lateral cyclic flapping, β_{1s}, fed to rotor lateral cyclic control, θ_{1c}:

The use of rotor lateral cyclic flapping as a feedback signal fed to rotor lateral cyclic control is unsatisfactory. It resulted in a reduction of the (RMS) value of lateral flapping at the expense of an increased (RMS) value of longitudinal flapping. The rate of change of lateral flapping is also an ineffective feedback signal configuration.

2. Multiple Feedback Loop Using a Single Control Effector Configuration

The previous section provides an overview of the performance to be expected using simple single feedback control configurations. The possibility of using combinations of the most promising of these can then be investigated. The use of combined feedback paths to a single controller are discussed in this section, and the use of more than one controller is discussed in the next section of the report. The general configuration for this type of system is shown by the mathematical block diagram of Figure III-17. As an example, two output quantities are indicated. These signals are multiplied by feedback static sensitivities and summed together to form the command signal to the control effector.

System 2-1. Bending displacement, q_1, and bending velocity $\dot{q}_1$, fed to the rotor longitudinal cyclic, θ_{1s}:

In light of the results presented in the previous section, an obvious configuration to examine is one that uses bending displacement feedback to longitudinal cyclic to increase bending stiffness and uses bending velocity feedback to improve the damping. Figure III-17 was drawn for this case. Since one output is the time derivative of the other, only one sensor would

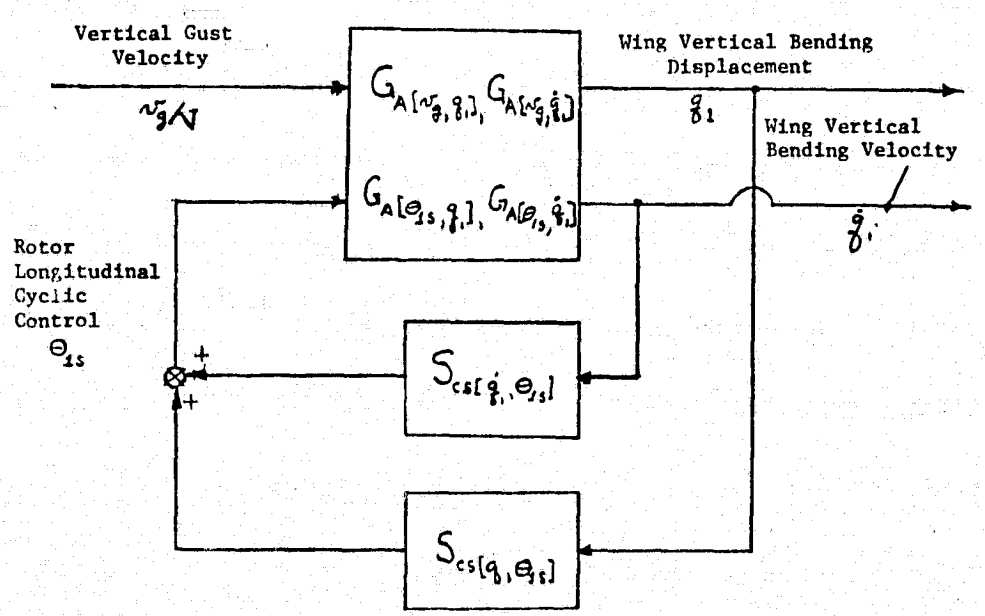

Figure III-17. Mathematical Block Diagram, Multiple Feedback, Single Control Effector System.

probably be required, and both signals would be obtained by proper signal processing. As noted in the previous section, the choice of feedback gains involved a compromise between reduction of wing vertical bending and reduction in rotor flapping. Depending upon that choice, the optimization program can then be used to obtain an optimized set of feedback loop static sensitivities.

As was noted in discussing system 1-1, the minimum (RMS) value of bending occurred at a value of the bending feedback static sensitivity which provided little gain margin with the critical mode being wing chordwise bending. Further, the use of wing bending velocity feedback alone added damping to the bending mode. The wing chordwise bending remained stable but with reduced damping, and the wing torsion mode became the critical mode. This feedback also amplified the rotor flapping. With those considerations in mind, Table III-1 summarizes the performance to be achieved with these feedback configurations. If the (RMS) value of wing bending is to be minimized, Row No. 5 of the table shows that the control system reduces the bending to 46% of the uncontrolled airplane response or a 54% reduction. To do this however, the (RMS) value of the flapping motions have increased by 60%. It is to be noted that the bending and bending rate feedback gains are limited by the approaching instability of the torsion mode. This mode contributes little to the (RMS) value of the response until the gains are increased to values at which instability is approached. A plot of (RMS) value versus gain would rise abruptly on the high gain side of the minimum point. Thus there is very little gain margin associated with the optimized set of gains, and for the case of Row 5, the gain margin is only 8%. Comparing Row No. 4 with No. 5 it is seen that the bending velocity feedback provides only a 3% gain in performance.

If the optimization criterion is taken to be minimization of flapping, Row No. 6 of the table indicates that lower bending feedback gains (by approximately a factor of 3) are required, and the longitudinal flapping has been reduced by 74%. The reduction in wing vertical bending is of the

No.	Feedback Static Sensitivities		(RMS) value closed loop / (RMS) value open loop		
	$S_{cs[q_1,\theta_{1s}]}$	$S_{cs[\dot{q}_1,\theta_{1s}]}$	$(RMS)q_1$	$(RMS)\beta_{1c}$	$(RMS)\beta_{1s}$
1	0	0	1.0	1.0	1.0
2	-4.046	0	0.68	0.31	0.53
3	0	-0.15 sec	0.78	1.03	1.07
4	-12.0	0	0.49	1.57	1.72
5	-12.0	-0.425	0.461	1.57	1.63
6	-4.046	-0.15	0.64	0.26	0.45

Open Loop Values (nondimensional): $(RMS)q_1 = 0.178$; $(RMS)\beta_{1c} = 0.590$; $(RMS)\beta_{1s} = 0.253$

Table III-1. Ratio of (RMS) Responses of Wing Vertical Bending, q_1, Rotor Longitudinal Cyclic Flapping, β_{1c}, and Rotor Lateral Cyclic Flapping, β_{1s}, Closed Loop to Open Loop Operation. System 2-1.

order of 36% rather than the 54% achieved with the higher gains.

For comparison purposes, the performance of the single feedback configurations, using the optimized values found for the flapping case, are also presented in Rows 2 and 3. Comparing 2 and 6 one observes that the bending rate feedback to the rotor has produced a rather marginal improvement in performance at this value of bending displacement feedback gain also. The (RMS) value of flapping is slightly lower when using the bending rate feedback, but several conflicting effects are operating here. First it was noted that when the bending displacement signal was used to counter the low frequency flapping due to the gust input, the bending mode contribution to the flapping response became relatively more important. Thus increasing the damping ratio of the bending mode would decrease that mode's contribution to the flapping when operating near the minimum flapping point. A second effect counteracts the first in that the bending velocity feedback was seen to amplify the low frequency component of flapping (see Figure III-8). Finally, the presence of the rate feedback does reduce the wing vertical bending response somewhat, which at the same value of displacement feedback gain to the cyclic would result in a lower (RMS) value of θ_{1s} and accordingly less correction of the flapping due to the gust. Thus the minimum flapping point occurs at a somewhat higher value of the displacement gain than if the bending rate feedback were not present. Figure III-18 presents the shaped pulse response for case No. 6, and this can be directly compared with the displacement feedback case, Figure III-5, to see the effect of the bending velocity feedback upon the time response. There is better damping of the bending, and the bending mode component appearing on the flapping response is reduced, but the excitation of the wing torsion mode is much more evident. These interactions would need to be evaluated further in deciding whether the complexity of the added feedback path were warranted.

System 2-2. Wing vertical bending, q_1, and bending velocity, $\dot{q}_1$, fed to the wing flap, δ_f:

The wing flap was found to be effective for reducing wing vertical

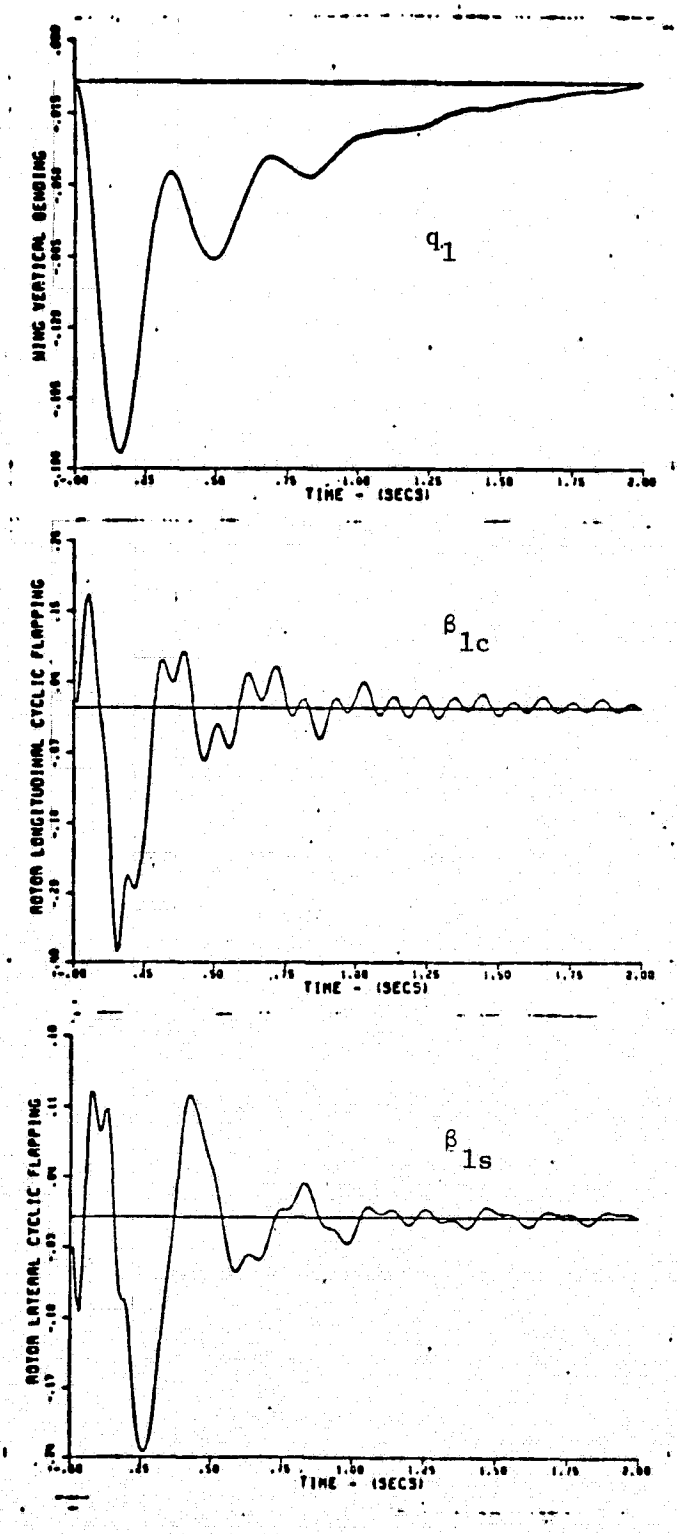

Figure III-18. System 2-1. Response to a Shaped Pulse of Vertical Gust Velocity. Case 6, Table III-1.

bending. By feeding the bending and bending rate signals to the flap, both the natural frequency and the damping ratio of the bending mode can be modified. This feedback structure is not particularly effective for reducing rotor flapping, and indeed if improvement in flapping performance is to be achieved the required algebraic sign of the feedback results in increased bending response (refer again to Figure III-12). When used to decrease bending response, the optimization of this configuration would call for generally increasing feedback gains. The stability characteristics of this configuration are good, and the system remains stable beyond the point at which the gain values reach impractically high values. The bending response can be reduced to the order of 41% using feedback gains of

$$S_{cs[q_1,\delta_f]} = -13.6 \qquad S_{cs[\dot{q}_1,\delta_f]} = -0.17 \text{ sec}^{-1}.$$

The flapping response is amplified by less than 3%. The shaped pulse response is shown in Figure III-19. Comparing this with the uncontrolled airplane response of Figure II-4, one sees that a large decrease in vertical bending has been achieved with little change in the rotor flapping characteristics.

System 2-3. Wing vertical bending, q_1, wing vertical bending velocity, $\dot{q}_1$, and rotor longitudinal flapping, β_{1c}, fed to the rotor longitudinal cyclic control, θ_{1s}:

A configuration obtained by adding a rotor flapping feedback path to the feedback configuration of design 2-1 was investigated to see if a further improvement in flapping response could be obtained. In optimizing the flapping response the following loop gains resulted:

$$S_{cs[q_1,\theta_{1s}]} = -3.67 \quad , \quad S_{cs[\dot{q}_1,\theta_{1s}]} = -0.145 \text{ sec}^{-1} \quad , \quad S_{cs[\beta_{1c},\theta_{1s}]} = 0.241$$

The corresponding ratios of closed loop (RMS) value to open loop value were:

Bending motion, q_1:	0.62
Rotor longitudinal flapping, β_{1c}:	0.23
Rotor lateral flapping, β_{1s}:	0.40

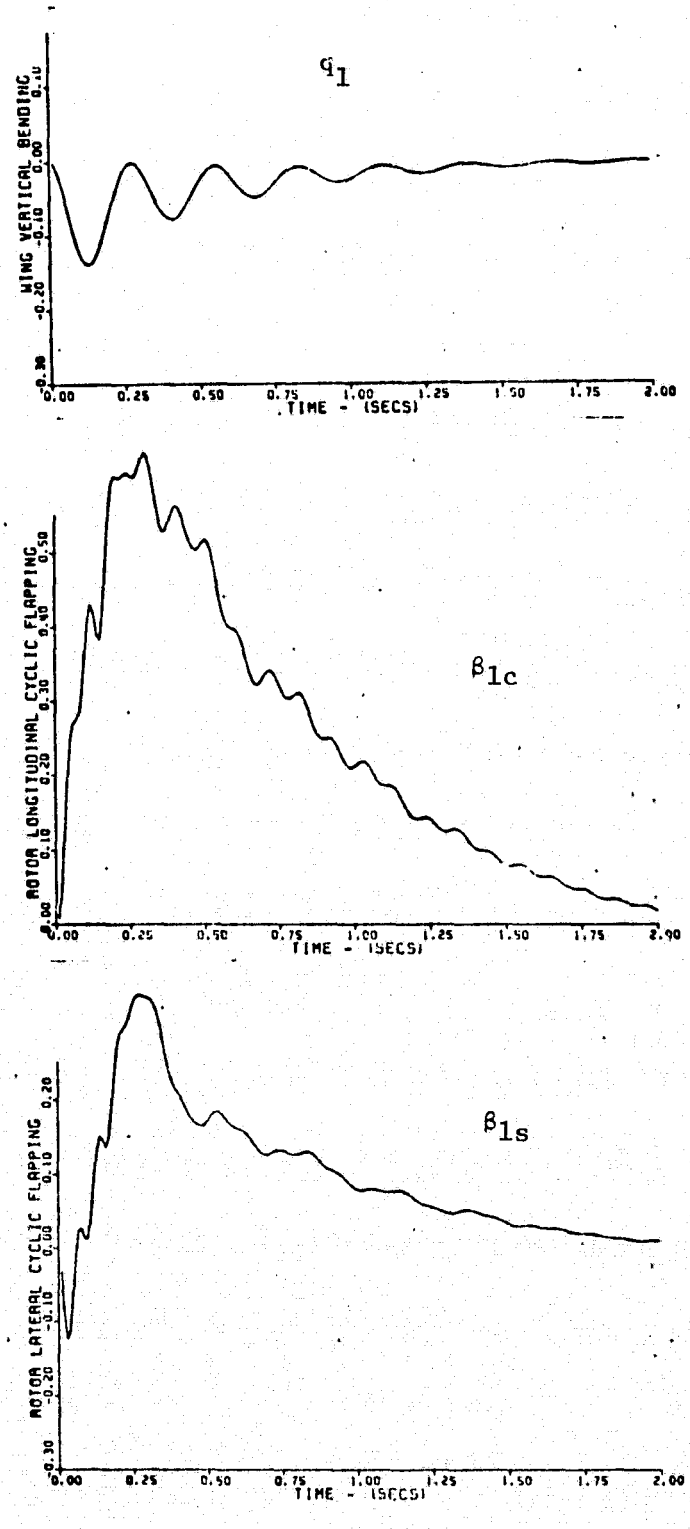

Figure III-19. System 2-2. Response to a Shaped Pulse of Vertical Gust Velocity.

This represents about a 10% improvement in flapping over system 2-1 with approximately the same bending response. The bending feedback static sensitivities were also 10% lower. These improvements are small considering the added complexity of the flapping feedback path.

3. Multiple Controllers

The previous discussion dealt with various feedback configurations which used a single control effector. Since there are several control effectors possible, one has further options of using feedback configurations of various kinds which feed information to more than one effector concurrently. On the basis of the previous results, only a few of the possible combinations are of practical interest. Figure III-20 presents the general arrangement using two controls and two output quantities as feedback signals.

System 3-1. Wing vertical bending displacement, q_1, and vertical bending velocity, $\dot{q}_1$, fed to both the rotor longitudinal cyclic control, θ_{1s}, and the wing flap, δ_f:

The rotor longitudinal cyclic control and the wing flap produce similar effects upon bending performance. Thus one would expect that the combination of these controls would permit a greater reduction in bending than either could produce alone for comparable feedback gains. For the configuration of Figure III-20, the output quantities become the wing vertical bending displacement and the bending velocity. These quantities are modified by the feedback static sensitivities, summed, and fed to the respective controls. There are four feedback gains to be selected. To minimize wing vertical bending, the optimization program tried to use as high gains as possible, with the limitation being the approach to instability of one of the high frequency modes of response. In this regard the presence of the feedbacks to the wing flap was sufficient to keep the wing chordwise bending mode stable (although with very little damping), and the critical mode became wing torsion. The critical feedback paths

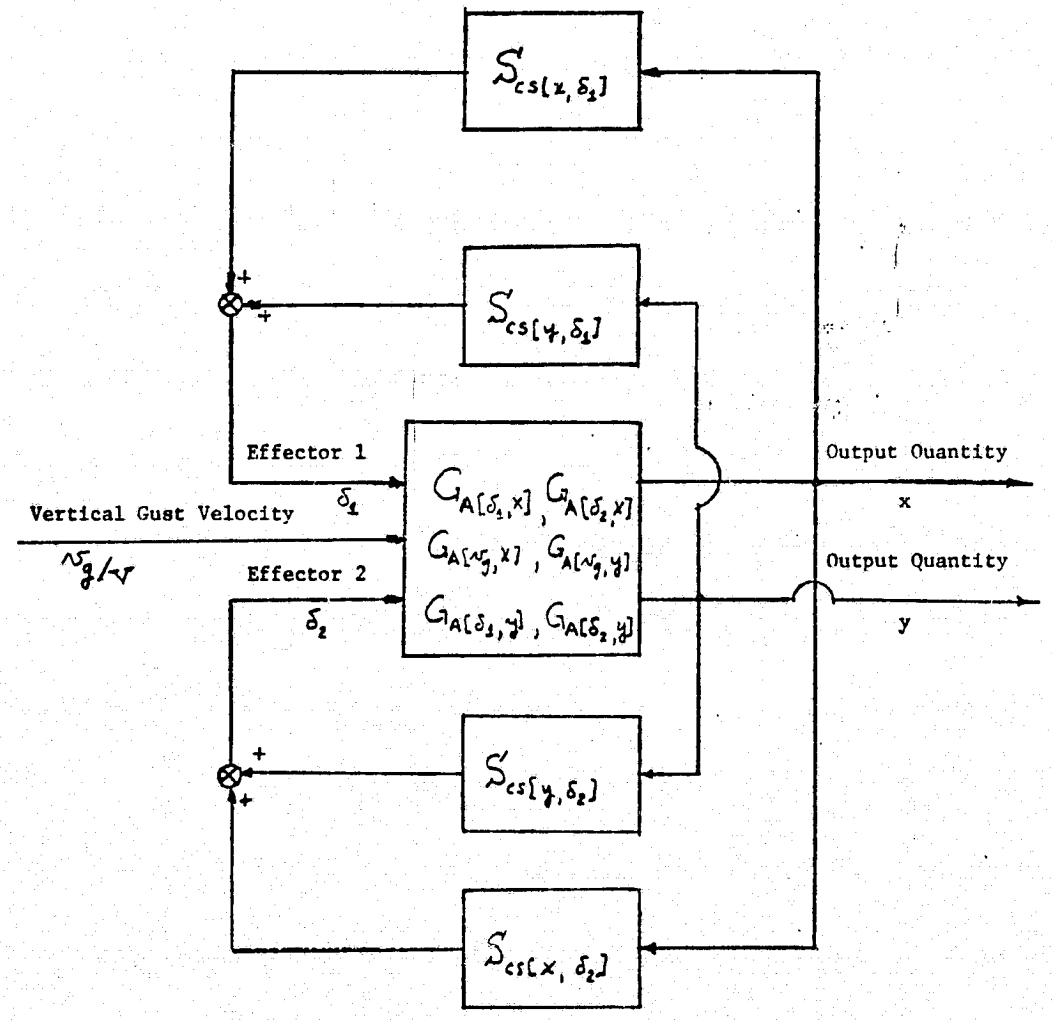

Figure III-20. Mathematical Block Diagram, Multiple Feedback, Multiple Control Effector System.

were those to the rotor longitudinal cyclic control.

If one minimized rotor blade flapping rather than wing bending, a well defined minimum point was obtained for the same reasons discussed previously with system 1-1. The bending rate feedback gain to the rotor longitudinal cyclic was small, and little reduction in performance resulted if that path was removed. The set of values for the remaining feedback path gains to minimize flapping were:

$$S_{cs[q_1,\theta_{1s}]} = -8.04 \quad , \quad S_{cs[q_1,\delta_f]} = -18.0 \quad , \quad S_{cs[\dot{q}_1,\delta_f]} = -0.179 \text{ sec.}$$

The ratios of closed-loop to open-loop values of (RMS) bending and flapping that result were

Wing vertical bending	(q_1)	0.28
Rotor longitudinal flapping	β_{1c}	0.17
Rotor lateral flapping	β_{1s}	0.22

The gain margin as determined by $S_{cs[q_1,\theta_{1s}]}$ is approximately 5. The bending performance is better than achieved with any of the previously investigated configurations. Figure III-21 presents the shaped pulse response for this case. Since these gains represented the minimum flapping point, increasing the gains would improve the bending performance with a deterioration in flapping performance, but the sensitivity of bending improvement with gain is low. Thus this configuration and these gain values may represent about the best performance that one could expect, and some of these gains may be impractically high. Since bending information is being fed to both controls, an appreciable component of the control response will be contributed by the bending mode. Since the sensitivity of the performance to the wing vertical bending velocity to wing flap feedback gain is low, one can increase that gain to improve the bending mode damping. Increasing this gain to 1.0 sec changed the control response due to a representative gust input from that shown in Figure III-21 to that in Figure III-22. Improved bending mode damping is seen to be accompanied by increased excitation of the torsion mode on the longitudinal flapping response. The (RMS) level of rotor longitudinal

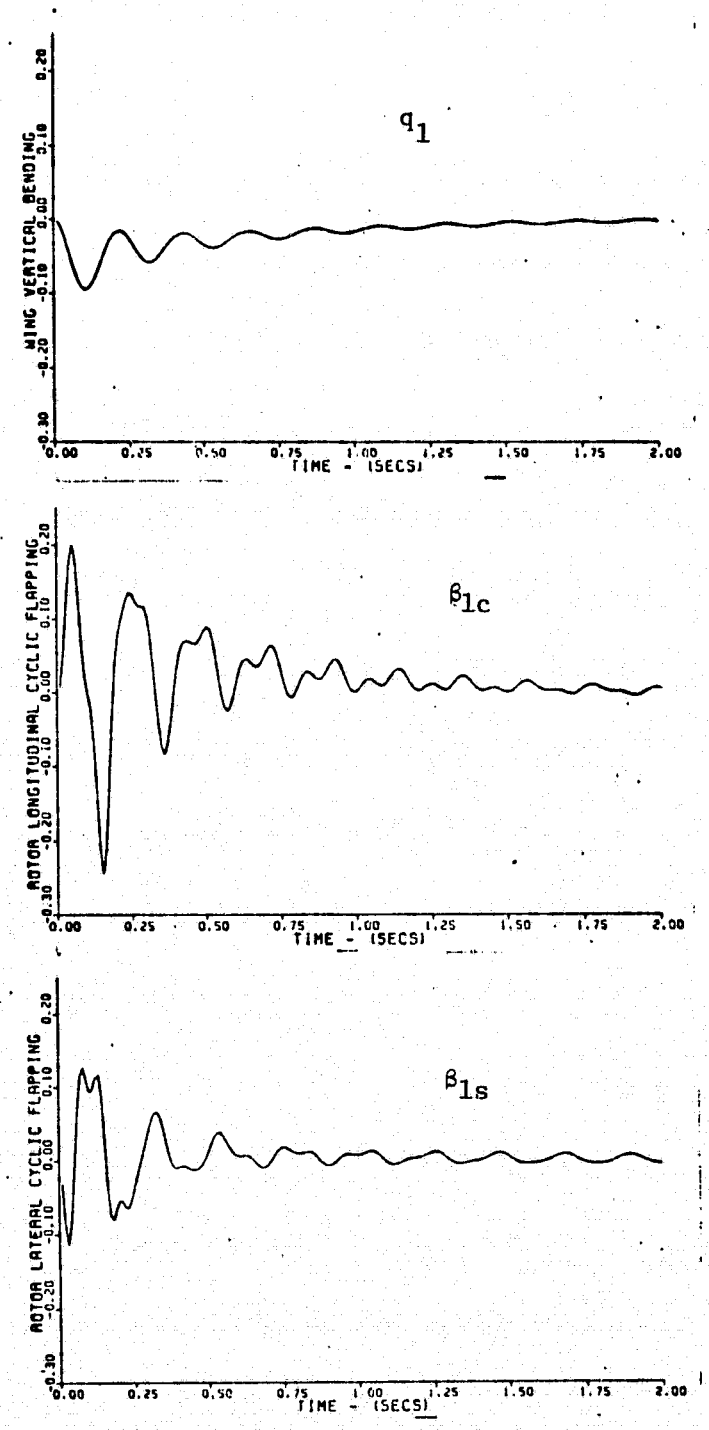

Figure III-21. System 3-1. Response to a Shaped Pulse of Vertical Gust Velocity.

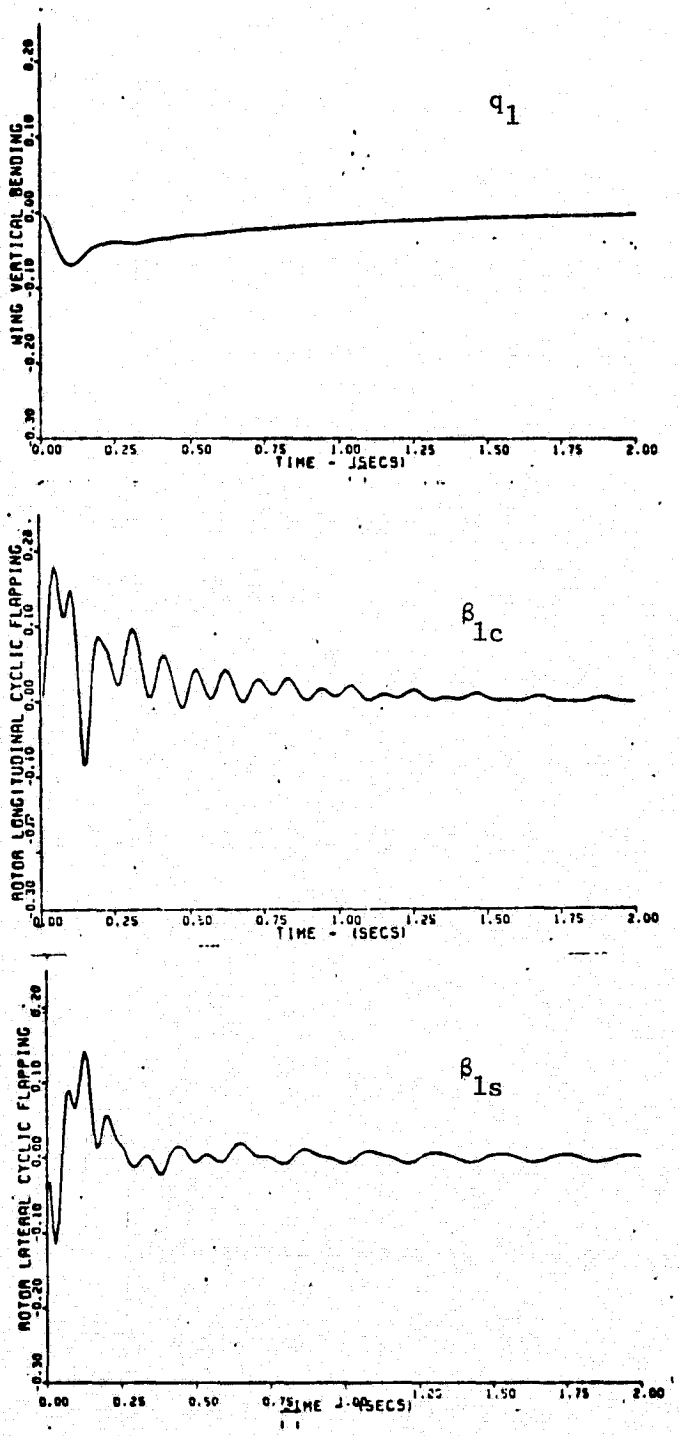

Figure III-22. System 3-1. Response to Shaped Pulse of Vertical Gust Velocity. Effect of Increased Bending Velocity Feedback.

flapping remained essentially the same while the level of rotor lateral flapping was reduced 50%. Although it has not been investigated further at this time, the separation of the frequency of the torsion mode would seem to permit effective filtering of that mode.

The sensitivity of performance to variation of the bending displacement to rotor cyclic feedback gain is shown in Figure III-23. The minimum flapping point is reached at a higher value of the bending to rotor longitudinal cyclic gain in this configuration than in system 1-1 because the feedbacks to the flap have increased the effective bending stiffness. Thus the low frequency component of flapping caused by the gust, which is countered by the low frequency component of the bending feedback to the rotor, requires a higher feedback gain to achieve the same performance. Figure III-23 reveals that the bending feedback to the rotor cyclic is primarily functioning to reduce the rotor blade flapping, and the bending improvement results from the feedback to the wing flap.

Comparing this configuration with system 2-2, one notes that if no feedbacks to the rotor are used, the $(RMS)q_1$ can be reduced to 34% using these gains to the flap. Therefore the added feedback to the rotor resulted in approximately another 6% improvement in performance. Looked at from a different viewpoint, the capability of a control configuration utilizing only the rotor blade longitudinal cyclic control (Row 2 to Table III-1) is only half that obtainable from using the wing flap control. Note however that other design constraints, such as reduced flap size, might reduce the relative advantage of the flap over the rotor. If one considers the variation of (RMS) bending with gain shown in Figure III-12 for system 1-4, one might estimate that the bending performance achieved with the multiple controller configuration would still be of the order of 50% with $S_{cs[q_1,\delta_f]}$ decreased by one half.

System 3-2. Addition of rotor longitudinal flapping displacement, β_{1c}, feedback to rotor longitudinal cyclic control, θ_{1s}, to the configuration of system 3-1:

By measuring the rotor blade flapping and feeding that signal to the

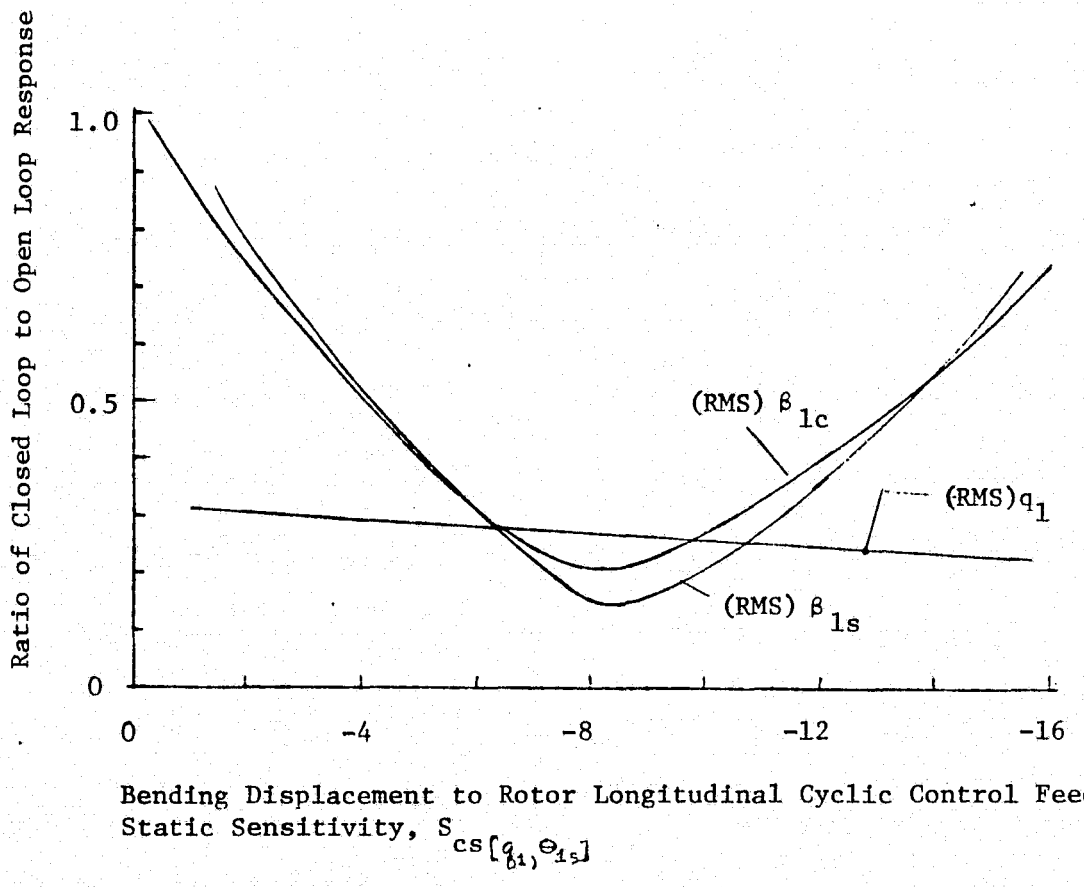

Figure III-23. System 3-1. Sensitivity of Performance to Variation in the Control System Feedback Sensitivity relating Rotor Longitudinal Cyclic Control to Wing Vertical Bending.

longitudinal cyclic control in addition to the feedback configuration of system 3-1, only a 5% improvement in flapping response was achieved with about a 10% reduction in the other loop gains. The bending response was somewhat worse, so that the increased complexity of this configuration provides only marginal benefit.

Chapter IV

EFFECT OF SERVO SYSTEM DYNAMICS

In Chapter III the servos needed to actuate the controls were assumed to be ideal in that dynamic lag and saturation effects were assumed to be negligible. If one includes a representation of the actual servo dynamic response characteristics, the effect is to introduce into the open loop transfer function a servo mode, or modes, which one would in general expect to produce dynamic lags that would be destabilizing. Saturation refers to the fact that there is a maximum power output of a servo, and the servo will not be able to follow input commands that call for power levels greater than that available. Typically this manifests itself in the servo reaching a maximum output velocity in an attempt to respond either to high frequency or to large magnitude inputs.

The dominant mode for hydraulic servos is often modelled as a first order lag component. Since no information is currently available as to the hardware characteristics of the servos in the prototype airplane, one could analyze the effects of the servo by presenting a sensitivity analysis of the performance as a function of the servo break frequency or bandwidth. There was insufficient time in this study phase to complete a definitive analysis of this type. However some preliminary results were obtained.

If one considers system 3-1 of Chapter III, it was found that as the bandwidth of the wing flap servo is decreased keeping the same control system gains, the chordwise bending mode becomes unstable at a bandwidth of approximately 10 cycles per second. As the bandwidth is decreased further, the chordwise bending mode becomes stable once more, and the wing vertical bending mode becomes unstable. At bandwidth less than 2 cycles/sec all modes are stable once more. It was also found that if the control system static sensitivity for bending velocity feedback to the wing flap were increased to 1.0 sec (a factor of 5), the system remained

stable over the entire range of bandwidth variation of the servo.

The effect of the servo upon the (RMS) response in turbulence has not been completely determined. Preliminary data indicates that for a practical servo bandwidth (greater than 10 cycle/sec) the wing vertical bending is affected very little provided control system gains are adjusted to insure stability. This is to be expected since the bandwidth of the turbulence spectrum is less than 0.5 cycle/sec. The effect upon rotor flapping can be greater than that upon the bending if the damping ratio of the modes becomes low, but compensation can be provided by increasing the bending velocity feedback gain as noted previously.

Therefore it is expected that the effect of servo dynamics can be minimized for the designs considered here. Any deterioration in performance can be offset by adjustment to the feedback gains. In fact the servo will provide some beneficial filtering of the higher frequency mode response of the system.

Chapter V

CONCLUSIONS AND RECOMMENDATIONS

A. Conclusions

The analytical studies of the capability of active control systems to reduce the (RMS) response of wing vertical bending displacement and rotor blade flapping during flight in atmospheric turbulence lead to the following conclusions:

1. Reduction in the (RMS) value of wing vertical bending displacement of the order of 50 to 75 per cent can be obtained with a feedback configuration that uses wing vertical bending displacement and velocity indications fed back to the rotor longitudinal cyclic control and to a symmetrically operable trailing edge wing flap. Reductions beyond that level of performance require an incremental increase in complexity per incremental improvement in performance that is excessive if one is to assure that the system is to be reliable and failsafe. The feedback of wing vertical bending velocity to the rotor cyclic is of marginal benefit, tends to destabilize the wing torsion mode, and therefore could be omitted.

2. For the mathematical modelling used in this report, the trailing edge wing flap is a more effective controller than the rotor blade cyclic control for reducing wing bending in that higher control system gains can be used while maintaining satisfactory gain margins. A 50% reduction in bending can be achieved using only the flap. However the assumed flap is large and overly sensitive, and the required gain levels may be impractically high. Depending upon one's assumptions for available control sizes and control authorities, either wing flap or rotor cyclic could achieve a 30 per cent reduction in bending using practical gain levels.

3. The reduction in flapping produced by feeding wing vertical bending

information to the longitudinal cyclic control results from the fact that the low frequency component of the bending is in phase with the gust input that caused the flapping disturbance. Increasing the bending feedback gains beyond the point at which the flapping due to the gust input has been corrected will cause the (RMS) level of flapping to increase again resulting in a minimum operating point. Since the minimum flapping response is low however, higher bending gains can theoretically be used in order to reduce the bending response, while not amplifying the flapping beyond the level of the uncontrolled airplane. In specifying a control system design one will need to establish the desired trade-off between reducing flapping and reducing wing vertical bending.

4. The primary factor contributing to the reduction in (RMS) level of bending and flapping is the low frequency components of the forced response over the bandwidth of the frequency spectrum of the gust input, (a bandwidth of 1.4 radian/sec) and not the transient components appearing at the natural frequencies of the wing-rotor response modes. Even though the (RMS) level of flapping has been reduced by feeding the bending signal to the cyclic control, the oscillatory component of the flapping response at the bending mode frequency is greatly amplified at the same time that the low frequency component is being reduced. The high frequency components contribute relatively little to the total (RMS) level so that increasing the damping of these oscillations results in only a slight decrease in the (RMS) value. If the oscillations are objectionable from the standpoints of wear or structural loads, however, one would need to provide filtering of the bending signal or to improve the damping ratio of the bending mode using bending velocity feedback to the wing flap. Feeding the bending velocity signal to the cyclic control to increase damping is limited in its effectiveness by its destabilizing effect upon the wing torsion mode.

5. If the wing vertical bending displacement signal is fed to the rotor blade longitudinal cyclic control, the chordwise bending mode becomes unstable as the loop gain is increased. As the gain is further increased, the wing chordwise bending mode becomes stable, and eventually the wing

torsion mode becomes unstable. When stable these modes contribute very little to the (RMS) value of wing bending. Thus a plot of (RMS) bending versus gain increases steeply as the critical gain is approached and then just as steeply returns to a generally decreasing trend until the next mode approaches instability. This can result in an optimization program giving a lower minimum value for the (RMS) bending with a system design that would be conditionally stable, even if one assumed that the higher gain levels would be practical to implement. The use of additional state variable feedback to stabilize a critical mode is not likely to avoid the parameter sensitivity problem for such a system. The uncertainties associated with mathematical modelling and the difficulties accompanying high control loop gains make such system designs unattractive.

6. In the absence of better quantitative specifications upon the desirability of reducing bending and flapping levels below the levels achievable with these relatively simple feedback configurations, the additional complexity of configurations utilizing more feedback paths than used in system 3-1 together with the redundancy that safety would require is not warranted.

7. Wing vertical bending velocity feedback to the rotor longitudinal cyclic control provides only marginal improvement in reducing bending and flapping, and it reduces the gain margin with respect to torsional mode instability.

8. Due to the low bandwidth of the power spectral density for the gust input, the control effector dynamic lag is not a limiting factor. Present state of the art actuators can be provided with sufficient bandwidth. The primary effect of the servo mode will be to require a higher bending velocity feedback gain to assure stability.

9. If an active control system is to be used, compensation to improve gain margins would be necessary in order to allow for the uncertainties

associated with the mathematical modelling of the wing/rotor system.

10. Of the two rotor blade cyclic controls, only the longitudinal cyclic is effective in reducing bending and flapping.

11. Measuring rotor blade flapping and feeding it back to the rotor cyclic control to reduce flapping is not as effective as feeding back wing vertical bending, and it tends to destabilize the wing torsion mode.

B. Recommendations

As a result of this investigation the following recommendations are made:

1. Inasmuch as a wind tunnel model of this wing/rotor system is available, a wind tunnel evaluation of these results should be performed. The model has servo actuators for controlling blade cyclic which have adequate bandwidth. While there are no trailing edge flaps on the model, there is a tip mounted flap used for response input testing which may provide a possible simulation of wing flap performance.

2. The benefits of an active control system for the complete full scale airplane should be quantitatively assessed so that the trade-off between benefit and cost could be established.

3. The sensitivity of the system design to flight condition variation needs to be determined.

4. If active controls are to be employed to increase the stability margin for those modes that approach instability at high speed, a sensitivity analysis assessing the effects of mathematical modelling inaccuracies and of design parameter tolerances should be performed. This would include consideration of chordwise random gust inputs as well as the vertical gust inputs.

5. The effects produced by the control system feedback paths during normal aircraft maneuvers including transition into and out of hover would need to be assessed.

6. Only a preliminary estimation of the type of sensor and sensor location has been made. It appears that an accelerometer with filtering can be used to provide bending information. Such a sensor responds to wing torsion also depending upon its chordwise location, and this may make it possible to use the chordwise location to help stabilize the torsion mode. It is to be noted that the wind tunnel uncontrolled tests have not indicated as much torsion mode response as the mathematical model predicts neglecting structural damping.

7. The use of active control systems for reducing (RMS) wing bending and rotor flapping levels for cruising flight through turbulence has been investigated in this report. Little attention has been devoted to the use of active controls for improving the stability margin variation with forward speed. This is an area of investigation that could be pursued.

8. The development of aerodynamic control effectors specifically designed to be efficient force producers for the purpose of reducing wing bending motions may be an area for future NASA research. This would separate such controls from the primary flight control system and would have accompanying safety advantages at the cost of added complexity.

Appendix A

AIRPLANE DATA

The data base for modelling the airplane wing/rotor assembly is that found in Reference 1 for the Bell proprotor designs. The rotor is a gimballed, stiff in-plane type with 3 blades. The wing semispan is 200 inches. The flight condition considered is 250 knots at sea level.

The state equations for wing/rotor assembly are given by Equation A-1. Following the results of Reference 1, nine modes of response are included resulting in an 18th order state vector. In Equation A-1, the state vector is partitioned into displacement and velocity vectors, and the 18 x 18 state matrix is then partitioned into four 9 x 9 matrices of which one is a null matrix and one is an identity matrix. The numerical values for the remaining two matrices are presented in Figure A-1. Five inputs are considered and the (9x5) input coefficient matrix is presented in Figure A-2.

State Equation:

$$\frac{d}{dt}\begin{bmatrix} \underline{x} \\ \dot{\underline{x}} \end{bmatrix} = \left[\begin{array}{c|c} 0 & I \\ \hline A_1 & A_2 \end{array}\right]\begin{bmatrix} \underline{x} \\ \dot{\underline{x}} \end{bmatrix} + \begin{bmatrix} 0 \\ B \end{bmatrix} \underline{u} \qquad \text{A-1)}$$

where

$$\underline{x}^T = [\beta_0, \beta_{1c}, \beta_{1s}, \zeta_0, \zeta_{1c}, \zeta_{1s}, q_1, q_2, p]$$

$$\underline{u}^T = [v_g/v, \delta_f, \theta_{1s}, \theta_0, \theta_{1c}]$$

0 = null matrix

I = identity matrix

Using the data presented in Figures A-1 and A-2, the transfer functions and step function residues were obtained. These are presented in Figure A-3.

The static sensitivity is the Bode gain. The residues are tabulated in the same order as the corresponding poles. From the residues, those modes receiving the greatest excitation can be identified. For an impulse input the magnitude of the step residue would be multiplied by the magnitude of the corresponding pole. Due to the particular form of data input to the computer program, the transfer functions list a cancelling pole-zero pair at the origin which can be ignored.

Figure A-4 presents closed loop transfer functions for system 3-1.

A_1 - matrix

-3.672	-.9642E-03	-.1333E-02	-.6621	.9162E-02	.6403E-03	-.5512E-04	1.006	.4790E-03
.9955E-04	.1328	-.3596	.3227E-03	.5164E-01	.2232	-.7205E-01	.5514	-1.793
-.1453	.3697	.1490	-.4711	-.3170	.4571E-01	.6749E-01	.7159	.3344
-.1258	-.5938E-03	-.8207E-03	-16.66	.5642E-02	.3943E-03	-.3394E-04	.6197	.2949E-03
.8675E-01	-.2272	.4411	.2812	-.8583	-.3973	-.1567E-02	-1.100	-.3979E-01
-.3256E-02	-.4494	-.2159	-.1055E-01	.4004	-.9265	-.4084	.1656E-01	-1.255
-.3696E-04	-.4341E-03	.9742E-03	-.1198E-03	.1019E-02	-.1024E-01	-.1218	.1937E-03	.3078E-03
.8681E-01	.4098E-03	.5664E-03	.2814	-.3894E-02	-.2721E-03	.2343E-04	-.4276	-.2034E-03
.9376E-04	-.1675E-01	.1045E-01	.3039E-03	.6068E-02	-.9673E-01	-.4630E-01	.5669E-03	-1.766

A_2 - matrix

-.5431	-.2592E-03	-.9248E-04	.2836	.1016E-02	.2487E-01	-.1258E-01	-.8009	-.6815E-01
.1414E-05	-.3717	-1.997	.5950E-06	.5992	-.1112E-01	.1992E-01	-5.113	.3431
-.2065E-02	2.000	-.3705	-.8686E-03	.7497E-03	.3412	-1.091	-.6059	-2.209
.1785	-.1597E-03	-.5694E-04	-.4372	.6258E-03	.1532E-01	-.7746E-02	-.1883	-.4197E-01
.1232E-02	.4404	.1027E-03	.5185E-03	-.3892	-2.011	-.8385E-01	.2232	-.4068
-.4625E-04	-.6097E-03	.4423	-.1946E-04	2.194	-.4022	.7270	-.2555E-01	.9778E-01
-.5252E-06	-.8537E-05	.2767E-03	-.2209E-06	.2646E-01	-.1065E-02	-.2435E-01	-.1515E-01	-.1370E-02
.1233E-02	.1102E-03	.3929E-04	.5188E-03	-.4319E-03	-.1057E-01	.5345E-02	.1218E-02	.2896E-01
.1332E-05	-.1218E-02	.2771E-02	.5604E-06	.2661	-.1073E-01	-.4838E-01	-1.469	-.2254E-01

Figure A-1. State Equation Coefficient Matrices for Wing/Rotor Assembly: 250 knots, sea level, gimballed rotor; frequency nondimensionalized by rotor rotational angular velocity of 48.9 rad/sec (458 RPM).

B - matrix

.1065E-02	.2368E-03	.1404E-03	.9036	-.3443E-02
-.1587E-01	-.4625E-01	.3812E-01	-.2662E-05	.6975
-.3334	.1683E-03	.6958	.3886E-02	-.2449E-02
.6559E-03	.1458E-03	.8642E-04	.1348	-.2120E-02
-.8026E-03	-.1122E-02	.7821E-03	-.2319E-02	-.8627
.3589	-.1227E-02	-.8374	.8704E-04	.8604E-03
-.1756E-01	.8609E-02	.3673E-02	.9883E-06	.1966E-04
-.4526E-03	-.1006E-03	-.5963E-04	-.2321E-02	.1463E-02
-.1207E-01	-.4728E-01	.3679E-01	-.2507E-05	.1804E-02

Figure A-2. Input Coefficient Matrix for the Wing/Rotor Assembly: 250 knots, sea level, gimballed rotor; frequency nondimensionalized by rotor rotational angular velocity of 48.9 rad/sec (458 RPM).

Output: Rotor Longitudinal Flapping, β_{1c}, (radian)

FOR INPUT NO. 1 OUTPUT NO. 2

STATIC SENSITIVITY = .77263

ZEROES

(1974.6 + .0 J)	(.0 + .0 J)	(-10.236 + 199.10 J)
(3.3913 + 121.27 J)	(-12.877 + 91.695 J)	(5.1845 + 64.169 J)
(-.31184 + 29.686 J)	(.70137 + 16.301 J)	(-3.8953 + 14.518 J)
(-15.561 + .0 J)	(-13.099 + .0 J)	

POLES

(.0 + .0 J)	(-10.232 + 199.08 J)	(-7.2509 + 118.42 J)
(-9.9139 + 95.089 J)	(-12.872 + 91.694 J)	(-1.5697 + 61.736 J)
(-.53121 + 29.556 J)	(-.73701 + 16.703 J)	(-5.4299 + 12.127 J)
(-13.785 + 2.0597 J)	(-15.545 + .0 J)	

POLAR FORM FOR IMPULSE RESIDUES,	(MAGNITUDE , PHASE)	(RAD/SEC , DEG)
(.0 , .0)	(.242308-03, 23.240)	(1.8126 , 52.781)
(6.9889 , 179.34)	(.17440E-01, 11.136)	(2.1843 , 111.12)
(.99523E-01, 145.29)	(.55065 , 102.76)	(3.0432 , 176.85)
(10.530 , 19.013)	(.10538 , 180.01)	

Output: Rotor Lateral Flapping, β_{1s}, (radian)

FOR INPUT NO. 1 OUTPUT NO. 3

STATIC SENSITIVITY = .30381

ZEROES

(.0 + .0 J)	(-10.211 + 199.08 J)	(-1.9305 + 120.68 J)
(-12.877 + 91.690 J)	(-.69571E-01+ 64.217 J)	(-32.673 + .0 J)
(.11781E-01+ 29.653 J)	(14.971 + .0 J)	(.66932 + 17.935 J)
(-9.9877 + 9.2787 J)	(-15.534 + .0 J)	

POLES

(.0 + .0 J)	(-10.232 + 199.08 J)	(-7.2509 + 118.42 J)
(-9.9139 + 95.089 J)	(-12.872 + 91.694 J)	(-1.5697 + 61.736 J)
(-.53121 + 29.556 J)	(-.73701 + 16.703 J)	(-5.4299 + 12.127 J)
(-13.785 + 2.0597 J)	(-15.545 + .0 J)	

POLAR FORM FOR IMPULSE RESIDUES,	(MAGNITUDE , PHASE)	(RAD/SEC , DEG)
(.0 , .0)	(.17269E-02, 172.60)	(3.0931 , 143.88)
(16.262 , 87.551)	(.23768E-01, 101.21)	(1.7106 , 51.148)
(.34609 , 43.316)	(2.1066 , 79.884)	(7.3976 , 97.290)
(24.140 , 87.335)	(.14749 , 180.01)	

Output: Wing Vertical Bending Coordinate, q_1 (radian)

FOR INPUT NO. 1 OUTPUT NO. 7

STATIC SENSITIVITY = -.14455

ZEROES

(.0 + .0 J)	(-10.234 + 199.09 J)	(-14.002 + 128.47 J)
(-6.2505 + 97.424 J)	(-12.843 + 91.661 J)	(-1.2009 + 63.369 J)
(-.51564 + 29.633 J)	(-5.8339 + 12.698 J)	(-10.065 + .0 J)
(-15.559 + .0 J)	(-12.982 + .0 J)	

POLES

(.0 + .0 J)	(-10.232 + 199.08 J)	(-7.2509 + 118.42 J)
(-9.9139 + 95.089 J)	(-12.872 + 91.694 J)	(-1.5697 + 61.736 J)
(-.53121 + 29.556 J)	(-.73701 + 16.703 J)	(-5.4299 + 12.127 J)
(-13.785 + 2.0597 J)	(-15.545 + .0 J)	

POLAR FORM FOR IMPULSE RESIDUES,	(MAGNITUDE , PHASE)	(RAD/SEC , DEG)
(.0 , .0)	(.241148-04, 110.14)	(.23644 , 128.67)
(.21021 , 38.124)	(.40133E-02, 53.252)	(.15116 , 74.067)
(.48299E-01, 84.518)	(10.156 , 86.015)	(1.2190 , 1.7695)
(2.0029 , 179.28)	(.20658E-01, .0)	

Figure A-3(a). Wing/Rotor Transfer Functions and Impulse Response Residues: Input - Vertical gust velocity, (v_g/V), (radian) 250 knots, sea level, frequency units - (radian/sec).

Output: Rotor Longitudinal Flapping β_{1c}, (radian)

FOR INPUT NO. 6 OUTPUT NO. 2

STATIC SENSITIVITY = -1.5742

ZEROES

(1691.6 + .0 J)	(.0 + .0 J)	(-10.234 + 199.09 J)
(5.0599 + 120.31 J)	(-12.792 + 91.671 J)	(6.3180 + 64.757 J)
(-.26465 + 29.834 J)	(-.33116 + 16.589 J)	(-3.6945 + 14.129 J)
(-15.552 + .0 J)	(-13.082 + .0 J)	

POLES

(.0 + .0 J)	(-10.232 + 199.08 J)	(-7.2509 + 118.42 J)
(-9.9139 + 95.089 J)	(-12.872 + 91.694 J)	(-1.5697 + 61.736 J)
(-.53121 + 29.556 J)	(-.73701 + 16.703 J)	(-5.4299 + 12.127 J)
(-13.785 + 2.0597 J)	(-15.545 + .0 J)	

POLAR FORM FOR STEP RESIDUES,	(MAGNITUDE , PHASE)	(, DEG)
(.0 , .0)	(.15957E-06, 42.766)	(.17341E-01, 151.63)
(.72921E-01, 33.561)	(.15139E-02, 17.827)	(.41378E-01, 18.194)
(.51810E-02, 63.893)	(.97464E-02, 14.188)	(.19931 , 59.401)
(.73354 , 152.11)	(.28100E-02, .0)	

Output: Wing Vertical Bending Coordinate, q_1, (radian)

FOR INPUT NO. 6 OUTPUT NO. 7

STATIC SENSITIVITY = .31931E-01

ZEROES

(.0 + .0 J)	(-29.464 + 218.52 J)	(-10.287 + 199.08 J)
(-1.8081 + 98.220 J)	(-12.887 + 91.757 J)	(-.20660 + 66.036 J)
(-.47812 + 29.886 J)	(-5.4309 + 13.816 J)	(-2.7103 + .0 J)
(-15.572 + .0 J)	(-13.647 + .0 J)	

POLES

(.0 + .0 J)	(-10.232 + 199.08 J)	(-7.2509 + 118.42 J)
(-9.9139 + 95.089 J)	(-12.872 + 91.694 J)	(-1.5697 + 61.736 J)
(-.53121 + 29.556 J)	(-.73701 + 16.703 J)	(-5.4299 + 12.127 J)
(-13.785 + 2.0597 J)	(-15.545 + .0 J)	

POLAR FORM FOR STEP RESIDUES,	(MAGNITUDE , PHASE)	(, DEG)
(.0 , .0)	(.83818E-06, 39.081)	(.20967E-01, 30.322)
(.20344E-01, 61.542)	(.42599E-03, 1.8781)	(.26840E-01, 20.023)
(.20817E-01, 5.4935)	(1.5378 , 165.07)	(.72542 , 119.82)
(1.2995 , 9.8714)	(.15995E-01, -180.01)	

Figure A-3(b). Wing/Rotor Transfer Functions and Step Response Residues: Input - Rotor Longitudinal Cyclic Deflection (radians) 250 knots, sea level, frequency units - (radian/sec).

Output: Rotor Longitudinal Flapping, β_{1c}; (radian)

```
FOR INPUT NO.  5 OUTPUT NO.  2
STATIC SENSITIVITY =  .10840E-01

ZEROES
( .0          + .0          J)    (-10.228      + 199.08      J)    (-2.5302      + 112.25      J)
(-24.120      + 102.87      J)    (-12.925      + 91.751      J)    (-.71636      + 38.516      J)
( 10.396      + .0          J)    (-4.0977      + 15.867      J)    (-5.9814      + 6.0279      J)
(-15.557      + .0          J)    (-13.112      + .0          J)

POLES
( .0          + .0          J)    (-10.232      + 199.08      J)    (-7.2509      + 118.42      J)
(-9.9139      + 95.089      J)    (-12.872      + 91.694      J)    (-1.5697      + 61.736      J)
(-.53121      + 29.556      J)    (-.73701      + 16.703      J)    (-5.4299      + 12.127      J)
(-13.785      + 2.0597      J)    (-15.545      + .0          J)

POLAR FORM FOR   STEP  RESIDUES,   (MAGNITUDE  ,  PHASE    )    (            ,  DEG    )
( .0          ,  .0          )    ( .92096E-05,  36.249    )    ( .64996E-01,  9.2926  )
( .26347      ,  152.58      )    ( .54179E-02,  91.259    )    ( 1.6833     ,  20.218  )
( .15307      ,  39.417      )    ( .92369     ,  174.90    )    ( .77263     ,  98.112  )
( 1.0365      ,  164.99      )    ( .82257E-02,  .0         )
```

Output: Rotor Lateral Flapping, β_{1s}, (radian)

```
FOR INPUT NO.  5 OUTPUT NO.  3
STATIC SENSITIVITY =  .39417E-02

ZEROES
( .0          + .0          J)    (-1052.4      + .0          J)    ( 399.43      + .0          J)
(-10.767      + 198.98      J)    ( 7.5424      + 120.51      J)    (-12.824      + 91.742      J)
(-43.869      + .0          J)    ( 1.2154      + 32.147      J)    ( 13.735      + .0          J)
(-11.111      + 10.026      J)    (-4.8683      + 4.8329      J)    (-15.537      + .0          J)

POLES
( .0          + .0          J)    (-10.232      + 199.08      J)    (-7.2509      + 118.42      J)
(-9.9139      + 95.089      J)    (-12.872      + 91.694      J)    (-1.5697      + 61.736      J)
(-.53121      + 29.556      J)    (-.73701      + 16.703      J)    (-5.4299      + 12.127      J)
(-13.785      + 2.0597      J)    (-15.545      + .0          J)

POLAR FORM FOR   STEP  RESIDUES,   (MAGNITUDE  ,  PHASE    )    (            ,  DEG    )
( .0          ,  .0          )    ( .12629E-03,  85.084    )    ( .12002     ,  100.18  )
( .66167      ,  114.65      )    ( .11516E-01,  103.96    )    ( 1.4226     ,  39.614  )
( .58594      ,  63.177      )    ( 3.7984     ,  162.40    )    ( 2.0329     ,  12.577  )
( 2.5635      ,  88.450      )    ( .12039E-01,  .0         )
```

Output: Wing Vertical Bending Coordinate, q_1, (radian)

```
FOR INPUT NO.  5 OUTPUT NO.  7
STATIC SENSITIVITY =  .70573E-01

ZEROES
( .0          + .0          J)    (-10.233      + 199.08      J)    (-7.2918      + 119.74      J)
(-9.3210      + 95.023      J)    (-12.859      + 91.713      J)    (-2.1439      + 59.297      J)
(-.57385      + 29.423      J)    (-5.5073      + 12.154      J)    (-13.908      + 2.0919      J)
(-15.544      + .0          J)

POLES
( .0          + .0          J)    (-10.232      + 199.08      J)    (-7.2509      + 118.42      J)
(-9.9139      + 95.089      J)    (-12.872      + 91.694      J)    (-1.5697      + 61.736      J)
(-.53121      + 29.556      J)    (-.73701      + 16.703      J)    (-5.4299      + 12.127      J)
(-13.785      + 2.0597      J)    (-15.545      + .0          J)

POLAR FORM FOR   STEP  RESIDUES,   (MAGNITUDE  ,  PHASE    )    (            ,  DEG    )
( .0          ,  .0          )    ( .22574E-07,  119.10    )    ( .24281E-03,  7.7110  )
( .22799E-03,  115.38      )    ( .10148E-04,  66.477    )    ( .33748E-02,  162.05  )
( .21244E-02,  162.09      )    ( .48906     ,  176.54    )    ( .88217E-02,  97.967  )
( .55492E-02,  179.02      )    ( .40409E-04,  .0         )
```

Figure A-3(c). Wing/Rotor Transfer Functions and Step Response Residues: Input - Wing Flap, Deflection (rad.) 250 knots, sea level, frequency units - radian/second.

(a) Output: Rotor Longitudinal Cyclic Flapping, β_{1c}

```
ACOF =  1.45253      17.6621      102.977      411.170      1145.75      2442.59      4548.85      5800.70

ACOF =  7856.40      6038.94      6147.05      2989.83      2311.13      710.531      424.570      75.2137

ACOF =  35.3962      2.64555      1.00000

BCOF =  .898012E-01  .472606      4.86670      23.2563      81.7715      233.543      262.788      632.760

BCOF =  228.198      510.028      83.7635      153.374      10.3224      17.8636      .212909      .615035

BCOF = -.158654E-01

CLOSED LOOP ROOTS
  (-.20950     + 4.0707     J)      (-.13915     + 2.4101     J)      (-.26644     + 1.9042     J)
  (-.21245     + 1.9370     J)      (-.37912E-01+ 1.2597      J)      (-.81820E-02+ .60988      J)
  (-.88393E-01+ .61156      J)      (-.12044     + .26032     J)      (-.25360     + .0         J)
  (-.22703     + .0         J)

CLOSED LOOP ZEROES
  ( 39.827     + .0         J)      (-.20960     + 4.0707     J)      (-.26671     + 1.9045     J)
  ( .72258E-01+ 2.4743      J)      ( .96589E-01+ 1.2875      J)      (-.95195E-02+ .61161      J)
  (-.26852     + .0         J)      (-.93474E-01+ .26016      J)      ( .14209E-01+ .17115      J)
```

(b) Output: Rotor Lateral Cyclic Flapping, β_{1s}

```
ACOF =  1.45253      17.6621      102.977      411.170      1145.75      2442.59      4548.85      5800.70

ACOF =  7856.40      6038.94      6147.05      2989.83      2311.13      710.531      424.570      75.2137

ACOF =  35.3962      2.64555      1.00000

BCOF =  .229497E-01  .139993      1.4E023      2.03643      -3.01735     -62.3901     -121.339     -266.617

BCOF = -371.385      -271.914     -299.335     -103.833     -87.8609     -14.7027     -9.92128     -.621703

BCOF = -.333419

CLOSED LOOP ROOTS
  (-.20950     + 4.0707     J)      (-.13915     + 2.4101     J)      (-.26644     + 1.9042     J)
  (-.21245     + 1.9370     J)      (-.37912E-01+ 1.2597      J)      (-.81820E-02+ .60988      J)
  (-.88393E-01+ .61156      J)      (-.12044     + .26032     J)      (-.25360     + .0         J)
  (-.22703     + .0         J)

CLOSED LOOP ZEROES
  (-.20917     + 4.0708     J)      (-.37630E-01+ 2.4661      J)      (-.26648     + 1.9044     J)
  (-.74756E-03+ 1.3079      J)      (-.68503     + .0         J)      (-.56851E-02+ .61488      J)
  ( .27525     + .0         J)      (-.17219     + .22723     J)      (-.35519E-01+ .13159      J)
```

Figure A-4. Closed-loop transfer functions. System 3-1. $S_{cs[q_1,\theta_{1s}]} = -8.04$, $S_{cs[q_1,\delta_f]} = -18.0$, $S_{cs[\dot{q}_1,\delta_f]} = -0.179$ sec.; Input: Vertical gust velocity.

(c) Output: Wing Vertical Bending Coordinate, q_1

```
ACOF =  1.45253      17.621      102.977      411.173      1145.75      2442.59      4548.85      5800.70
ACOF =  7856.40      6038.94     3147.35      2966.83      2311.13      710.531      424.570      75.2137
ACOF =  35.3962      2.64555     1.00000

BCOF = -.829873E-01 -.993016    -5.36325     -19.1433     -44.6175     -72.1686     -115.627     -90.5692
BCOF = -105.632      -48.9436    -41.3637     -12.0567     -7.77338     -1.28468     -.635114     -.449906E-01
BCOF = -.175607E-01

CLOSED LOOP ROOTS
(-.20950     + 4.0707    J)    (-.13915     + 2.4101    J)    (-.25641     + 1.9042    J)
(-.21245     + 1.9370    J)    (-.379123-01+ 1.2557     J)    (-.818203-02+ .60388     J)
(-.88393E-01+ .61156     J)    (-.12044     + .26032    J)    (-.25360     + .0        J)
(-.22703     + .0        J)

CLOSED LOOP ZEROES
(-.20951     + 4.0708    J)    (-.28598     + 2.6267    J)    (-.12781     + 1.9918    J)
(-.26670     + 1.9044    J)    (-.239862-01+ 1.2901     J)    (-.123852-01+ .61076     J)
(-.11925     + .25966    J)    (-.20572     + .0        J)    (-.26505     + .0        J)
```

Note: ACDF ≡ denominator polynomial coefficients in increasing order of Laplace operator

BCDF ≡ numerator polynomial coefficients

Figure A-4 (continued)

APPENDIX B. COMPUTER PROGRAM

Algorithm for Computing the Root Mean Square Value

Given a transfer function G, relating a gust input to an output quantity of the tilt-rotor,

$$G(p) = K \frac{\prod_{j=1}^{m} (p-z_i)}{\prod_{i=1}^{m} (p-p_i)} \quad , \tag{B-1}$$

where $\prod$ denotes the product operation, and a von Karman gust Power Spectral Density (ASD), see Reference 2.

$$(PSD)v_g = \frac{\sigma^2_L}{2\pi V} \frac{1 + \frac{8}{3}[1.339(L/V)]^2}{\left\{1 + [1.339(L/V)]^2\right\}^{11/6}} \tag{B-2}$$

$$\approx \frac{\sigma^2_L}{2\pi V} \frac{1 + \frac{8}{3}(\frac{1.339 \quad L}{V})^2}{[1 + (1.339 \frac{L}{V})^2]^2} = \frac{\sigma^2_L b^4}{2\pi V a^2} \frac{(p + a)(p - a)}{(p + b)^2 (p - b)^2}$$

where

$$b = \frac{V}{1.339L} \quad , \qquad a = \sqrt{\frac{3}{8}}\, b$$

The mean square response is given by:

$$\sigma^2 = \int_{-\infty}^{\infty} G(j\omega)\, G(-j\omega)\, (PSD)v_g \, d\omega$$

$$= \frac{1}{j} \int_{-\infty}^{\infty} dp \, \frac{c(p)\, c(-p)}{d(p)\, d(-p)} \tag{B-3}$$

where

$$d(p) = \prod_{i=1}^{n} (p-p_i) \quad (p+b)^2$$

$$c(p) = \left(K \frac{\sigma^2 L\, b^4}{2\eta V\, a^2} \right)^{1/2} \prod_{j=1}^{m} (p - z_j) \quad (p + a)$$

According to Reference 3 the infinite integral can be computed simply by a partial fraction expansion of $\frac{c(p)\ c(-p)}{d(p)\ d(-p)}$ into (2n+4) modes of which half are in the left half plane and half are in the right half plane. Numerical integration can thus be avoided.

Let

$$f(p) \triangleq \frac{c(p)c(-p)}{d(p)d(-p)} = \sum_{i=1}^{n} \frac{R_i}{p-p_i} + \sum_{i=n+1}^{2n} \frac{R_i}{p-p_i} + \frac{R_{2n+1}}{p+b} + \frac{R_{2n+2}}{(p+b)^2} + \frac{R_{2n+3}}{p-b} + \frac{R_{2n+4}}{(p-b)^2}$$

where $p_{n+i} = - p_i$ for $i = 1, 2, \ldots, n$

and

$$R_i = \lim_{p \to p_i} (p-p_i)\ f(p) \quad i = 1, 2, \ldots, n$$

$$R_{2n+1} = \lim_{p \to -b} \frac{d}{dp} \left[(p+b)^2 \frac{c(p)c(-p)}{d(p)d(-p)} \right]$$

$$R_{2n+2} = \lim_{p \to -b} (p+b)^2\ f(p)$$

$$R_{2n+3} = \lim_{p \to b} \frac{d}{dp} \left[(p-b)^2\ f(p) \right]$$

$$R_{2n+4} = \lim_{p \to b} (p-b)^2\ f(p)$$

Equation B-3 then becomes

$$\frac{1}{j}\int_{-j\infty}^{j\infty} dp\left(\sum_{i=1}^{n}\frac{R_i}{p-p_i}+\frac{R_{2n+1}}{p+b}\quad\frac{R_{2n+2}}{(p+b)^2}\right)$$

$$=\mathcal{L}^{-1}\left(\sum_{i=1}^{n}\frac{R_i}{p-p_i}+\frac{R_{2n+1}}{p+b}+\frac{R_{2n+2}}{(p+b)^2}\right)\Bigg|_{t=0}$$

$$=\sum_{i=1}^{n}R_i+R_{2n+1}$$

and

$$\int_{-j\infty}^{j\infty} dp\left(\sum_{i=1}^{n}\frac{R_i}{p-p_i}+\frac{R_{2n+1}}{p+b}+\frac{R_{2n+2}}{(p+b)^2}\right)$$

$$=\int_{-j\infty}^{j\infty} dp\left(\sum_{i=n+1}^{2n}\frac{R_i}{p-p_i}+\frac{R_{2n+1}}{p-b}+\frac{R_{2n+2}}{(p-b)^2}\right)$$

Consequently,

$$\sigma^2=2\left(\sum_{i=1}^{n}R_i+R_{2n+1}\right) \qquad \text{(B-4)}$$

The root mean square response then is

$$(\text{RMS})q=\sigma$$

As suggested by Reference 3, the value for the gust characteristic length, L, ranges from 400 to 500 feet. For a value of L = 422 ft, (V/L) = 1.0 and the power spectral density from equation B-2 is

$$(PSD)v_g = \frac{\sigma_{v_g}^2}{2\pi} \frac{(1 + p/0.457)}{(1 + p/0.747)^2} \qquad \text{B-5}$$

This power spectral density was used in calculating the (RMS) levels of system response to turbulence in this report.

NOTATION

A,B	-	state equation matrices
a,b	-	dummy variables used to denote gust spectrum break frequencies (see App. B).
G(p)	-	transfer function
I	-	identity matrix
K	-	root locus gain factor
L	-	gust characteristic length
0	-	null matrix
p	-	wing torsion coordinate, torsional angular deflection of the wing tip section. Positive nose up.
p	-	Laplace operator
(PSD)	-	denotes power spectral density
q_1	-	wing vertical bending coordinate, vertical bending deflection of the wing tip, nondimensionalized by the wing semi-span. Positive upward.
q_2	-	wing chordwise bending coordinate, chordwise bending deflection of the wing tip, nondimensionalized by the wing semi-span. Positive forward.
$S_{i[x,y]}$	-	static sensitivity of a component or system; the ratio of the incremental change in the output in response to an incremental change in the input under static or steady state conditions where i is a subscript identifying the component, x identifies the input, and y identifies the output. (S is same as the Bode gain factor.)
t	-	time in seconds
$\underline{x}$	-	state vector (n x 1)
v_g	-	vertical gust velocity, positive down
V	-	airplane airspeed

Greek Symbols

β_o - rotor blade collective flapping coordinate. In-phase component of the structural flapping deflection of the tip of the rotor blades, nondimensionalized by radius of the rotor. Positive forward for cruist flight.

β_{1c} - rotor blade longitudinal cyclic flapping coordinate. Cosine component of the out of phase flapping angle of rotation of the blade as a rigid body. Positive forward for cruist flight.

β_{1s} - rotor blade lateral cyclic flapping coordinate. Sine component of the out of phase flapping angle of rotation of the blade as a rigid body. Positive forward for cruise flight.

δ - general control effector displacement

δ_f - wing flap angular deflection from trim

σ - root mean square value

σ_w - standard deviation of random gust input

θ_o - rotor blade collective pitch angle. Rotation of the blades of the rotor in phase about the blade spanwise axis of rotation. Positive rotation increases rotor thrust.

θ_{1c} - rotor blade lateral cyclic angle. Cosine component of the out of phase rotation of the blades about the blade spanwise axis of rotation. Positive rotation increases lift of the blade.

θ_{1s} - rotor blade longitudinal cyclic angle. Sine component of the out of phase rotation of the blades about the blade spanwise axis of rotation. Positive rotation increases lift of the blade.

ω - general frequency variable, (rad/sec)

ω_n - undamped natural frequency of a second order mode (rad/sec)

ζ - damping ratio of a second order mode

ζ_o - rotor blade collective lagging coordinate. In-phase component of the in-plane deflection of the blade tip, nondimensionalized by the radius of the rotor. Positive in direction of rotation.

ζ_{1c} - rotor blade cosine cyclic lagging coordinate. Cosine component of the out of phase component of the in-plane deflection of the blade tip, nondimensionalized by the radius of the rotor. Positive in the direction of rotation.

ζ_{1s} - rotor blade sine cyclic lagging coordinate. Sine component of the out of phase component of the in-plane deflection of the blade tip, nondimensionalized by the radius of the rotor. Positive in the direction of rotation.

REFERENCES

1. Yasui, M., A Study of Gust Response for a Rotor-Propeller in Cruising Flight, MIT Aeroelastic and Structures Research Laboratory, NASA Contractor Report CR-137537, August 1974.

2. Frick, J.K. and Johnson, W., Optimal Control Theory Investigation of Proprotor/Wing Response to Vertical Gust, Ames Research Center and U.S. Army Air Mobility R & D Laboratory, NASA Technical Memorandum TMX-62384, Sept. 1974.

3. Newton, G.C., Gould, L.A., and Kaiser, J.F., Analytical Design of Linear Feedback Controls, John Wiley and Sons, New York, 1957.